

# Exploiting Degeneracy in Belief Propagation Decoding of Quantum Codes

Kao-Yueh Kuo\* and Ching-Yi Lai†

*Institute of Communications Engineering, National Yang Ming Chiao Tung University, Hsinchu 30010, Taiwan.*

Quantum information needs to be protected by quantum error-correcting codes due to imperfect quantum devices and operations. One would like to have an efficient and high-performance decoding procedure for quantum codes. A potential candidate is Pearl’s belief propagation (BP), but its performance suffers from the many short cycles inherent in quantum codes, especially *highly-degenerate* codes (that is, codes with many low-weight stabilizers). A general impression exists that BP cannot work for topological codes, such as the surface and toric codes. In this paper, we propose a decoding algorithm for quantum codes based on quaternary BP but with additional memory effects (called MBP). This MBP is like a recursive neural network with inhibition between neurons (edges with negative weights) during recursion, which enhances the network’s perception capability. Moreover, MBP exploits the degeneracy of quantum codes so that it has a better chance to find the most probable error or its degenerate errors. The decoding performance is significantly improved over the conventional BP for various quantum codes, including quantum bicycle codes, hypergraph-product codes, and surface (or toric) codes. For MBP on the surface and toric codes over depolarizing errors, we observe thresholds of 14.5%–16% and 14.5%–17.5%, respectively.

Keywords: belief propagation, sparse-graph quantum codes, degeneracy, surface and toric codes, threshold.

## I. INTRODUCTION

To demonstrate an interesting quantum algorithm, such as Shor’s factoring [1], a quantum computer needs to implement more than  $10^{10}$  logical operations, which means that the error rate of each logical operation must be much less than  $10^{-10}$ . With limited quantum devices and imperfect operations [2, 3], quantum information needs to be protected by quantum error-correcting codes to achieve fault-tolerant quantum computation [4, 5]. If a quantum state is encoded in a stabilizer code [6, 7], information about an occurred error, called *error syndrome*, can be measured without disturbing the quantum information of the state. Quantum stabilizer codes based on sparse graphs, such as topological codes (e.g., toric or surface codes [8, 9] and color codes [10]), random sparse-graph codes (e.g., bicycle codes) [11], and (generalized) hypergraph-product (GHP) codes [12, 13], are favorable since they afford two-dimensional layouts or simple quantum error correction procedures.

For a general stabilizer code, the decoding problem of finding the most probable error with the given error syndrome is very hard [14, 15] and an efficient decoding procedure with good performance is desired. The complexity of a decoding algorithm is usually measured in terms of the length  $N$  of a quantum code. Minimum-weight matching (MWM) [16] can be applied to decode a surface or toric code [17–20], and in this application, the complexity of MWM can be improved from  $O(N^4)$  to  $O(N^2)$  [21, 22]. Renormalization group (RG) uses a recursive strategy analogous to the decoding of concatenated codes to decode a toric (or surface) code with complexity proportional to  $N \log(\sqrt{N})$  [23]. Both MWM and

RG can be generalized for color codes [24]. On the other hand, most sparse quantum codes can be well decoded by belief propagation (BP) [11, 25–27] or its variants [28]. In particular, BP has nearly linear complexity  $O(Nj\tau)$  [27, 29], where  $j$  is the mean column-weight of the check matrix and should be much less than  $N$ ;  $\tau$  is the average number of iterations and  $\tau = O(\log \log N)$  is usually good enough for BP convergence [30, 31].

Although BP seems to have the lowest complexity, a long-standing problem in quantum coding theory is that BP does not perform well on quantum codes with *high degeneracy*. (We say that a code has *high degeneracy* or is *highly-degenerate* if it has many low-weight stabilizers compared to its minimum distance.) A stabilizer code has its Tanner graph inevitably containing many short cycles [11, 32], which deteriorate the message-passing process in BP, especially for codes with high degeneracy [33–35]. Any message-passing or neural network decoder may have this issue. Previously this issue is handled with additional efforts in pre-training by neural networks [36–39] or post-processing by the ordered statistics decoding [33, 34]. In addition, their decoders treat Pauli  $X$  and  $Z$  errors separately, which may incur additional overhead or performance loss. In this paper we will address this long-standing BP problem by devising a quaternary BP decoding algorithm with memory effects, abbreviated *MBP*, so that the degeneracy of quantum codes can be exploited.

A hard-decision decoding for classical codes is like an energy-minimization problem in a neural network (NN) associated with the code structure [40], where the energy function with discrete variables measures the parity-check satisfaction (denoted by  $J_S$ ). BP has been used as a tool to minimize the energy in statistical physics [31, 32, 41]. Moreover, an iterative decoder based on gradient decent optimization of the energy was proposed in [42, Sec. IV]. This motivate us to consider a soft-decision generalization of the energy function in [40], with vari-

\* kykuo@nycu.edu.tw

† cylai@nycu.edu.tw

ables that are log-likelihood ratios, and show that BP decoding of quantum codes in log domain [27] is to minimize the energy function. Our energy function has an additional term  $J_D$  that measures the distance between a data point and the initial channel statistics. Then we show that BP is like a gradient descent optimization for this generalized energy function but with more elegant step updates. Hence conventional BP works well for a nondegenerate quantum code as in the classical case.

For a highly-degenerate quantum code, it has many low-weight stabilizers corresponding to local minimums in the energy topology so that conventional BP easily gets trapped in these local minimums near the origin (cf. Fig. 2 for the details). This suggests that we should use a larger step (which can be controlled by message normalization [27]), but this is exactly contrary to the classical case that a small step is preferred for better convergence. Moreover, every degenerate error of the target error suffices to be the decoding target. Using larger steps may find these degenerate errors. However, this is simply not enough since larger steps may lead the decoding to diverge. An observation from neural networks is that *inhibition* (edges with negative weights) between neurons enhances the perception capability of a network, improving the pattern-recognition accuracy [43–47]. Our MBP is naturally formulated to have this inhibition function, which provides a memory effect that helps to resist wrong beliefs passed on the Tanner graph (wrong dependency in the messages [30]) or effectively accelerate the search in gradient descent. The complete algorithm of MBP will be provided in Sec. IIID, which is based on our previous work [25–27]. Consequently, MBP is a version of quaternary BP for Pauli errors  $\{I, X, Y, Z\}$  and only scalar messages are required. Since there is no additional computation, the complexity of MBP remains the same as conventional BP with necessary message normalization.

The performance of MBP can be further improved by choosing an appropriate step-size for each error. However, it is difficult to precisely determine the step-size. If the step-size is too large, MBP may return incorrect solutions or diverge. We propose to choose the step-size from an  $\varepsilon$ -net as in [48, 49]. The overall complexity is still  $O(Nj\tau)$  since the chosen  $\varepsilon$  is independent of  $N$ .

Another technique used in MBP is *fixed initialization* [50, 51]. The channel statistics is used to define the energy function and hence defines the energy topology. If MBP performs well on a certain channel statistics, it means that MBP can correctly determine most syndrome and error pairs on that topology. Thus it is better to keep this topology regardless of the true channel statistics.

Computer simulations of MBP on several quantum codes are performed. Although MBP naturally extends to a joint decoding of data-syndrome errors like [52], as a preliminary study of improving BP decoding on highly-degenerate codes without pre-training of post-processing, we consider to decode various kinds of codes with perfect syndrome measurements in this paper. We will first do a case study on the five-qubit code [53] to show how the

TABLE I. The thresholds of various decoders on surface codes ( $\epsilon_{\text{surf}}$ ) and toric codes ( $\epsilon_{\text{toric}}$ ) over depolarizing errors. An entry is denoted  $--$  if the data is not provided in the literature. The computation complexity of each decoder for surface/toric codes is also provided.

decoder	$\epsilon_{\text{surf}}$	$\epsilon_{\text{toric}}$	complexity
MWM [16]	15.5% [20]	15.5% <sup>a,b</sup> [18]	$O(N^2)$ [21]
RG-BP [23]	--	16.4%	$O(N \log N)$
MPS [55]	17%–18.5%	--	$O(N^2)$
UF [56]	--	14.85% <sup>a</sup>	$O(N)$
BP-MWM [57]	17.76% <sup>b</sup>	17.76%	$O(N^{2.5})$
MBP (this paper)	14.5%–16%	14.5%–17.5%	$O(N \log \log N)$

- a) If only the threshold of a decoder over bit-flip errors is provided, we rescale it by the factor  $\frac{3}{2}$  [11, Eq. (40)].
- b) It is usually considered that  $\epsilon_{\text{surf}} \leq \epsilon_{\text{toric}}$ . Figure 10 in [20] seems to suggest  $\epsilon_{\text{toric}} = 15\% < \epsilon_{\text{surf}} = 15.5\%$  according to the intersection points. However, the MWM threshold on toric codes over bit-flip errors is estimated to be 0.1031 [18], which, after rescaled by  $\frac{3}{2}$ , matches  $\epsilon_{\text{toric}} = 15.5\%$  finally claimed in [20]. Figures 10 and 12 in [57] seem to confusingly suggest  $\epsilon_{\text{toric}} = 17.76\% < \epsilon_{\text{surf}} = 17.84\%$  by the intersection points, so a single threshold value 17.76% was concluded in [57].

memory effect helps the gradient descent optimization. Then we decode quantum bicycle codes [11], a GHP code in [33], and (rotated) surface or toric codes [9].

Quantum bicycle codes have good error-correction performance and low decoding complexity but they may have high error-floor if there are many low-weight stabilizers [11, Fig. 6], which occurs if the generator vector of a bicycle code has low weight. A bicycle code has fixed stabilizer weight. When a code has fixed stabilizer weight, the weight is called *row-weight*. A bicycle code has its minimum distance upper bounded by its row-weight. However, the performance of BP depends more on the weight distribution of codewords [30, 31], rather than the code distance. We simulate the cases in [11, Fig. 6] and each error-floor is significantly improved using MBP. In particular, the average number of iterations is reduced, especially when the row-weight is small (i.e., when the code is more degenerate).

Next, we consider an  $[[N, K, D]] = [[822, 48, 16]]$  GHP code constructed in [33] with row-weight 8. Since the row-weight is less than the code distance, the code is highly-degenerate so the energy topology is hard for conventional BP to have good convergence. In [33], a decoding algorithm, called *BP-OSD- $\omega$* , is proposed based on BP with post-processing by ordered statistics decoding (OSD), together with a post-selection on  $2^\omega$  possible errors. The considered GHP code can be well decoded by BP-OSD- $\omega$  with  $\omega = 15$  so that degenerate errors can be found. However, OSD has subroutines of sorting, Gaussian elimination, and classical re-encoding [54] and the overall complexity of BP-OSD- $\omega$  is quite high. On the other hand, MBP with proper step-size achieves a similar decoding performance without any post-processing.

Finally we consider the decoding *threshold* on surface

codes ( $\epsilon_{\text{surf}}$ ) and toric codes ( $\epsilon_{\text{toric}}$ ) as a benchmark [17]. For depolarizing errors, the theoretical threshold of the surface or toric codes has an upper bound around 18.9% [48, 58, 59]. (This upper bound could be approached by a decoder based on Monte Carlo sampling methods [48, 58] with impractical complexity.) In the following, we compare decoders with practical complexity. MWM achieves  $\epsilon_{\text{surf}} \approx \epsilon_{\text{toric}} = 15.5\%$  [18, 20]. RG combined with BP (RG-BP) achieves  $\epsilon_{\text{toric}} = 16.4\%$  [23]. A decoder based on matrix product states (MPS) achieves  $17\% \leq \epsilon_{\text{surf}} \leq 18.5\%$  [55] (which has complexity  $O(N^2)$  like MWM but is more complex in practice since MPS needs many matrix operations). MBP achieves  $14.5\% \leq \epsilon_{\text{surf}} \leq 16\%$  and  $14.5\% \leq \epsilon_{\text{toric}} \leq 17.5\%$ , which improves the known thresholds in the case with complexity  $O(N \log N)$  or lower. Recently, decoders based on union-find (UF) [56] and BP-assisted MWM (BP-MWM) [57] were proposed, which are also efficient without complex pre-training or post-processing. The thresholds and complexity of various decoders are provided in Table I. Note that, as in remarked b) of Table I, the performance of a surface code is usually worse than its corresponding toric code, since a toric code does not have boundary qubits and its check matrix has a strong symmetry. The surface and toric codes have mean column-weight  $j \leq 4$  [8, 9]. Hence the complexity of MBP is  $O(Nj\tau) = O(N \log \log N)$ , since  $\tau = O(\log \log N)$  is good enough for MBP convergence (which will be observed in the empirical results) like the BP decoding of classical codes [30, 31].

Our simulation results show that MBP significantly improves the decoding performance of conventional BP. In particular, degeneracy is exploited so that degenerate errors may be returned by the decoder. It is known that BP can be treated as a recurrent neural network (RNN) [38, 49]. Similarly, our MBP induces an RNN with inhibition without the pre-training process. This may provide an explanation why RNN decoders (which may contain many negative-weight edges after training) work well on degenerate codes.

This paper is organized as follows. In Sec. II, we introduce stabilizer codes and the decoding problem. In Sec. III, we interpret the decoding problem as energy minimization and introduce our MBP algorithm. We also show the RNN induced by MBP and link it with the inhibition technique in Hopfield nets. In Sec. IV, we provide the computer simulation results for MBP decoding on various quantum codes. Finally we conclude and discuss some future research topics in Sec. V.

## II. PRELIMINARIES

### A. Stabilizer codes

We consider errors that are tensor product of Pauli matrices  $\{I = \begin{bmatrix} 1 & 0 \\ 0 & 1 \end{bmatrix}, X = \begin{bmatrix} 0 & 1 \\ 1 & 0 \end{bmatrix}, Y = \begin{bmatrix} 0 & -i \\ i & 0 \end{bmatrix}, Z = \begin{bmatrix} 1 & 0 \\ 0 & -1 \end{bmatrix}\}$ . In particular, we will simulate independent depolarizing errors with rate  $\epsilon$  so that each qubit independently

suffers a Pauli error  $I, X, Y$ , or  $Z$  with probability

$$(p^I, p^X, p^Y, p^Z) = (1 - \epsilon, \epsilon/3, \epsilon/3, \epsilon/3), \quad (1)$$

respectively. The *weight* of an  $N$ -fold Pauli operator in  $\{I, X, Y, Z\}^{\otimes N}$ , regardless of the global phase, is the number of its non-identity components. For small  $\epsilon$ , Pauli errors of lower weight occur with higher probability and we would like to mitigate their effects. In the following, the notation of tensor product  $\otimes$  will be omitted if no confusion arises in our discussion.

A *stabilizer group*  $\mathcal{S}$  is an Abelian subgroup of  $\{1, -1\} \times \{I, X, Y, Z\}^{\otimes N}$  such that  $-I^N \notin \mathcal{S}$ . Assume that  $\mathcal{S}$  has a set of  $N - K$  independent generators  $\{S_m\}_{m=1}^{N-K}$ . For simplicity, consider  $S_m \in \{I, X, Y, Z\}^{\otimes N}$ , though a generated element may still have negative phase. A binary  $[[N, K, D]]$  *stabilizer code* defined by  $\mathcal{S}$  is the  $2^K$ -dimensional subspace in  $\mathbb{C}^{2^N}$  that is the joint  $(+1)$ -eigenspace of  $\mathcal{S}$  [6, 7]. The parameter  $D$  is called the *minimum distance* of the code and will be defined below. The elements in  $\mathcal{S}$  are called *stabilizers*. Two Pauli operators either commute or anticommute with each other. If a Pauli error anticommutes with certain stabilizers, measuring those stabilizers will return eigenvalues  $-1$ . Consider the measurement result  $\pm 1$  to be mapped by  $+1 \mapsto 0$  and  $-1 \mapsto 1$ . Hence the measured eigenvalues of  $\{S_m\}_{m=1}^{N-K}$ , after mapping, are called the *error syndrome* of the error and a nonzero error syndrome suggests a detected error. Since a stabilizer has no effect on the code space, an error that is a stabilizer is harmless. Thus the minimum distance of the stabilizer code defined by  $\mathcal{S}$  is the minimum weight of a Pauli error that is harmful but cannot be detected. Let

$$N(\mathcal{S}) = \{E \in \{I, X, Y, Z\}^{\otimes N} : EF = FE \ \forall F \in \mathcal{S}\}. \quad (2)$$

Then  $D = \min_{F \in N(\mathcal{S}) \setminus \mathcal{S}} (\text{weight of } F)$ .

For  $F \in \mathcal{S}$  and a Pauli error  $E$ , the Pauli error  $EF$  and  $E$  are equivalent on the code space and hence  $EF$  is called a *degenerate error* of  $E$ . A quantum code is said to be *degenerate* if there are stabilizers of weight less than its minimum distance; otherwise, it is *nondegenerate*. An  $[[N, K, D]]$  stabilizer code has  $N - K$  independent stabilizer generators. We judge how degenerate a quantum code is by the percentage of its maximum number of independent stabilizer generators of weight less than  $D$ . Roughly speaking, we say that a code is *highly-degenerate* or has *high degeneracy* if this percentage is high. For example, a surface or toric code of  $D \geq 5$  is highly-degenerate since it is straightforward to find a set of  $N - K$  independent generators of weight  $\leq 4$  [8, 9].

For better decoding performance of BP,  $M \geq N - K$  stabilizers  $\{S_m\}_{m=1}^M$  will be measured [60]. For an error  $E = E_1 E_2 \cdots E_N \in \{I, X, Y, Z\}^{\otimes N}$ , we define its *binary syndrome vector*  $z = (z_1 z_2 \cdots z_M) \in \{0, 1\}^M$  by

$$z_m = \sum_{n=1}^N \langle E_n, S_{mn} \rangle \mod 2, \quad (3)$$

where the bilinear form  $\langle F_1, F_2 \rangle = 0$ , if two Pauli operators  $F_1$  and  $F_2$  commute, and  $\langle F_1, F_2 \rangle = 1$ , otherwise. For convenience, we form an  $M \times N$  *check matrix*

$$S = [S_{mn}] \in \{I, X, Y, Z\}^{M \times N},$$

where we decompose the stabilizer  $S_m$  into  $S_m = S_{m1}S_{m2} \cdots S_{mN} \in \{I, X, Y, Z\}^N$  for  $m = 1, 2, \dots, M$ . The *row-weight* of a row of  $S$  is referred to as the weight of its corresponding stabilizer.

**Definition 1** For an  $N$ -qubit code with minimum distance  $D$ , let  $r \times \text{BDD}$  denote the bounded distance decoding (BDD) of the code so that any Pauli error of weight no larger than  $\lfloor \frac{rD-1}{2} \rfloor$  is correctable. We say that  $r \times \text{BDD}$  has correction radius  $\lfloor \frac{rD-1}{2} \rfloor$ .

We use BDD to denote  $1 \times \text{BDD}$  for simplicity. Usually a good decoding procedure on a classical code has correction radius between  $\lfloor \frac{D-1}{2} \rfloor$  and  $\lfloor \frac{2D-1}{2} \rfloor$ . However, the degeneracy of a quantum code is not considered in BDD; we may have decoding performance much better than that in the quantum case. In addition, since we do not know how to estimate the exact channel fidelity for large quantum codes,  $r \times \text{BDD}$  serves as a good benchmark.

## B. BP decoding of quantum codes

Codes based on low-density parity-check (LDPC) matrices (also known as sparse-graph codes) achieves near channel-capacity performance in classical coding theory [30, 31]. The parity-check matrix of a code can be depicted as a Tanner graph, which is a bipartite graph containing variable nodes and check nodes, connected properly by edges [61, 62]. Belief propagation (BP) on the Tanner graph iteratively passes messages between the nodes so that an estimate of the marginal distribution of each coordinate of the error can be approximated [63, 64].

Consider an  $M \times N$  check matrix  $S$ . The relations between a Pauli error operator and its syndrome bits can be depicted by a Tanner graph with  $N$  variable nodes (corresponding to the  $N$ -fold Pauli error to be estimated) and  $M$  check nodes (corresponding to the given binary syndrome vector) such that an edge  $(m, n)$  (corresponding to  $S_{mn}$ ) connects variable node  $n$  and check node  $m$  whenever  $I \neq S_{mn} \in \{X, Y, Z\}$  [25, 32]. Figure 1 illustrates the Tanner graph for a check matrix  $S = \begin{bmatrix} X & Y & I \\ Z & Z & Y \end{bmatrix}$ .

Given a syndrome vector  $z \in \{0, 1\}^M$ , the decoding problem is to find the most probable Pauli error in  $\{I, X, Y, Z\}^N$  or one of its degenerate errors. A quaternary BP ( $\text{BP}_4$ ) algorithm computes an approximated marginal distribution  $\hat{P}(E_n = W | z) = q_n^W$  for  $W \in \{I, X, Y, Z\}$  for  $n = 1, 2, \dots, N$  in linear domain [25] and outputs  $\hat{E} = (\hat{E}_1, \hat{E}_2, \dots, \hat{E}_N)$  such that

$$\hat{E}_n = \arg \max_{W \in \{I, X, Y, Z\}} \hat{P}(E_n = W | z).$$

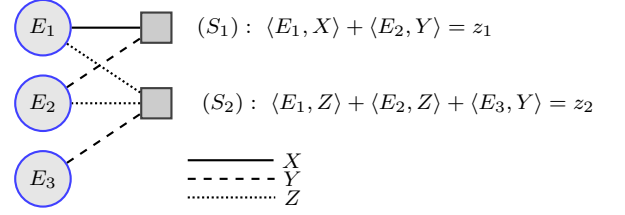


FIG. 1. The Tanner graph for  $S = \begin{bmatrix} X & Y & I \\ Z & Z & Y \end{bmatrix}$ . There are three variable nodes (represented by circles), two check nodes (represented by squares), and three types of edges.

This can also be done with log-likelihood ratios (LLRs)

$$\Gamma_n^X = \ln \frac{q_n^I}{q_n^X}, \quad \Gamma_n^Y = \ln \frac{q_n^I}{q_n^Y}, \quad \text{and} \quad \Gamma_n^Z = \ln \frac{q_n^I}{q_n^Z} \quad (4)$$

in log domain [27]. If the syndrome of  $\hat{E}$  matches  $z$ , then the decoder will output  $\hat{E}$ . This can be efficiently calculated by iteratively passing *scalar messages* on the Tanner graph in linear domain [25, 26] or log domain [27].

In this paper we will discuss  $\text{BP}_4$  in log domain with an LLR vector  $\Gamma = (\Gamma_1, \Gamma_2, \dots, \Gamma_N) \in \mathbb{R}^{3N}$  with  $\Gamma_n = (\Gamma_n^X, \Gamma_n^Y, \Gamma_n^Z) \in \mathbb{R}^3$  for  $n = 1, 2, \dots, N$ . (See Algorithm 1 in Sec. IIID, which is referred to as  $\text{MBP}_4$ . A conventional LLR- $\text{BP}_4$  is a special case of Algorithm 1 with  $\alpha = 1$  and  $\beta = 0$  there). There are two types of messages iteratively passed on each edge  $(m, n)$  connecting variable node  $n$  and check node  $m$ . Let  $\mathcal{M}(n)$  denote the set of neighboring check nodes of variable node  $n$  and  $\mathcal{N}(m)$  denote the set of neighboring variable nodes of check node  $m$ . (In other words,  $\mathcal{N}(m)$  is the support of  $S_m$ .) We will simplify a notation  $\mathcal{M}(n) \setminus \{m\}$  as  $\mathcal{M}(n) \setminus m$ . A *variable-to-check* message  $\lambda_{S_{mn}}(\Gamma_{n \rightarrow m})$  from variable node  $n$  to check node  $m$  carries the log-likelihood ratio that  $E_n$  commutes or anticommutes with  $S_{mn}$ , where  $\Gamma_{n \rightarrow m} = (\Gamma_{n \rightarrow m}^X, \Gamma_{n \rightarrow m}^Y, \Gamma_{n \rightarrow m}^Z)$  is the LLR of  $E_n = I$  to  $E_n = W$ , for  $W \in \{X, Y, Z\}$ , respectively, according to the messages from the other nodes  $m' \in \mathcal{M}(n) \setminus m$  and the function  $\lambda_W : \mathbb{R}^3 \rightarrow \mathbb{R}$  is defined as

$$\lambda_W(\gamma^X, \gamma^Y, \gamma^Z) \triangleq \ln \frac{1 + e^{-\gamma^W}}{e^{-\gamma^X} + e^{-\gamma^Y} + e^{-\gamma^Z} - e^{-\gamma^W}}.$$

On the other hand, suppose that  $S_{mn} \neq I$  and, by Eq. (3), we have a check bit relation

$$\langle E_n, S_{mn} \rangle = z_m + \sum_{n' \in \{1, 2, \dots, N\} \setminus n} \langle E_{n'}, S_{mn'} \rangle \pmod{2}.$$

Consequently a *check-to-variable* message  $\Delta_{m \rightarrow n}$  from check node  $m$  to variable node  $n$  will tell us the log-likelihood ratio of whether  $E_n$  commutes or anticommutes with  $S_{mn}$ . More precisely,

$$\Delta_{m \rightarrow n} = (-1)^{z_m} \bigoplus_{n' \in \mathcal{N}(m) \setminus n} \lambda_{S_{mn'}}(\Gamma_{n' \rightarrow m}), \quad (5)$$

where for a set of  $k$  real scalars  $a_1, a_2, \dots, a_k \in \mathbb{R}$ , the operation  $\boxplus$  is defined by

$$\boxplus_{n=1}^k a_n = 2 \tanh^{-1} \left( \prod_{n=1}^k \tanh \frac{a_n}{2} \right).$$

Then  $\Gamma_n$  is updated according to  $\Delta_{m \rightarrow n}$  for all  $m \in \mathcal{M}(n)$  and the initial distribution of  $E_n$ .

The BP algorithm iteratively updates the LLR of the marginal distributions  $\{\Gamma_n\}_{n=1}^N$  according to the passed messages on the Tanner graph. If the Tanner graph has no cycles, BP will compute the exact marginal distributions [62–66]. If there are not many short cycles, the approximation is usually very good [62, 65, 66].

Here we discuss a four-cycle example that needs some strategies from improvement. We refer the readers to [25–27] for more details about refined BP decoding algorithms for quantum codes, where the techniques of *message normalization* and *message scheduling* can be applied to improve the performance of BP. For example, given  $S = \begin{bmatrix} X & Y \\ Z & Z \end{bmatrix}$  and  $z = (1, 0)$ , it is difficult for a parallel-scheduled BP to determine whether the error is  $ZI$  or  $IZ$ , provided that they occur with the same probability. Poulin and Chung suggested to use BP with heuristic post-processing like random perturbation to have opportunity to converge to  $ZI$  or  $IZ$  [32]. However, with a non-parallel schedule (e.g., a serial schedule) and properly enlarged message magnitude (e.g., by message normalization), BP suffices to directly reach a decision. We will adopt this strategy in this paper.

### III. BP DECODING AS ENERGY MINIMIZATION

A classical decoding problem can be considered as an energy function minimization problem [40]. Given the error syndrome, the energy function is defined with respect to the parity checks so that each error vector matching the syndrome can be considered as a local minimum of the energy function. An iterative decoding algorithm can be used to find a local minimum of the energy function with an initial point defined by the channel statistics [42]. In particular, a decoding algorithm based on gradient optimization was proposed in [42].

We would like to characterize the energy function minimization problem for BP decoding of quantum codes. The energy function is defined on  $\mathbb{R}^{3N}$ , where each point represents the LLRs in Eq. (4). Instead of using only the energy defined by parity checks [40, 42], we introduce an additional term regarding the distance between a data point and the channel statistics. Then we explain why conventional BP fails to solve this energy function minimization problem for quantum codes with high degeneracy. To solve the problem, we introduce our MBP<sub>4</sub>.

#### A. Energy function of a BP decoding

Assume that qubit  $n$  undergoes a Pauli error with rate  $(p_n^I, p_n^X, p_n^Y, p_n^Z)$ , where  $p_n^I + p_n^X + p_n^Y + p_n^Z = 1$ . Let  $\Lambda_n = (\Lambda_n^X, \Lambda_n^Y, \Lambda_n^Z)$  for  $n = 1, 2, \dots, N$ , where

$$\Lambda_n^X = \ln \frac{p_n^I}{p_n^X}, \quad \Lambda_n^Y = \ln \frac{p_n^I}{p_n^Y}, \quad \text{and} \quad \Lambda_n^Z = \ln \frac{p_n^I}{p_n^Z}. \quad (6)$$

The channel statistics vector  $\Lambda = (\Lambda_1, \dots, \Lambda_N) \in \mathbb{R}^{3N}$  is the channel information we have before decoding. For depolarizing errors with rate  $\epsilon$ , we have  $(p_n^I, p_n^X, p_n^Y, p_n^Z) = (1 - \epsilon, \epsilon/3, \epsilon/3, \epsilon/3)$  and hence  $\Lambda_n^X = \Lambda_n^Y = \Lambda_n^Z = \ln \frac{1-\epsilon}{\epsilon/3}$ .

Suppose that the syndrome vector  $z = (z_1, \dots, z_M) \in \{0, 1\}^M$  is determined from stabilizer  $S_m = \otimes_{n=1}^N S_{mn}$  for  $m = 1, \dots, M$ . Then we define the energy function of the decoding problem with respect to the stabilizers  $\{S_m\}_{m=1}^M$  and the syndrome vector  $z$  as

$$J(\Gamma) = J_D(\Gamma) + \eta J_S(\Gamma), \quad (7)$$

where

$$J_D(\Gamma) = \frac{1}{2} \|\Gamma - \Lambda\|_2^2$$

and

$$J_S(\Gamma) = - \sum_{m=1}^M 2 \tanh^{-1} \left( (-1)^{z_m} \prod_{n \in \mathcal{N}(m)} \tanh \left( \frac{\lambda_{S_{mn}}(\Gamma_n)}{2} \right) \right) \quad (8)$$

for some  $\eta > 0 \in \mathbb{R}$ . (The value of  $\eta$  does not matter in the following discussion and will be postponed to discuss in Appendix C.)

The second term  $J_S(\Gamma)$  measures the satisfaction of each stabilizer and is similar to the case in [42, Sec. IV]. The additional term  $J_D(\Gamma)$ , which is convex in  $\Gamma$ , measures the distance between a point  $\Gamma \in \mathbb{R}^{3N}$  and the channel statistics  $\Lambda$ . This is critical since the initial channel statistics  $\Lambda$  affects the performance of BP [50] and this should be reflected in the energy function. An interpretation is that an logical error would lead to larger  $J_D$ .

#### B. Gradient decent optimization

Next we show that BP decoding is like a gradient decent minimization of the corresponding energy function Eq. (7). This provides a better understanding of how BP works.

One can easily verify that  $\nabla J = \left( \frac{\partial J}{\partial \Gamma_1^X}, \frac{\partial J}{\partial \Gamma_1^Y}, \frac{\partial J}{\partial \Gamma_1^Z}, \dots, \frac{\partial J}{\partial \Gamma_N^X}, \frac{\partial J}{\partial \Gamma_N^Y}, \frac{\partial J}{\partial \Gamma_N^Z} \right)$  has

$$\begin{aligned} \frac{\partial J}{\partial \Gamma_n^W} &= \Gamma_n^W - \Lambda_n^W \\ &+ \sum_{\substack{m \in \mathcal{M}(n) \\ S_{mn}=W}} \frac{\eta g_{mn}(\Gamma) e^{-\Gamma_n^W}}{1 + e^{-\Gamma_n^W}} \tilde{\Delta}_{m \rightarrow n} \\ &- \sum_{\substack{m \in \mathcal{M}(n) \\ (W, S_{mn})=1}} \frac{\eta g_{mn}(\Gamma) e^{-\Gamma_n^W}}{e^{-\Gamma_n^X} + e^{-\Gamma_n^Y} + e^{-\Gamma_n^Z} - e^{-\Gamma_n^{S_{mn}}}} \tilde{\Delta}_{m \rightarrow n}, \end{aligned} \quad (9)$$

where

$$g_{mn}(\Gamma) = \frac{1 - \tanh^2 \frac{\lambda_{S_{mn}}(\Gamma_n)}{2}}{1 - \left( \prod_{l \in \mathcal{N}(n)} \tanh \frac{\lambda_{S_{ml}}(\Gamma_l)}{2} \right)^2} > 0, \quad (10)$$

and

$$\tilde{\Delta}_{m \rightarrow n} = (-1)^{z_m} \prod_{n' \in \mathcal{N}(m) \setminus n} \tanh \frac{\lambda_{S_{mn'}}(\Gamma_{n'})}{2}. \quad (11)$$

Note that  $\tilde{\Delta}_{m \rightarrow n}$  in Eq. (11) and  $\Delta_{m \rightarrow n}$  in Eq. (5) are similar but different in two aspects. First, the function  $\tanh^{-1}$  in  $\Delta_{m \rightarrow n}$  does not change the sign of its argument but simply resizes it. Second,  $\Gamma_{n'}$  used in Eq. (11) and  $\Gamma_{n' \rightarrow m}$  used in Eq. (5) differ by a term  $\langle W, S_{mn} \rangle \Delta_{m \rightarrow n}$  as shown in Eq. (15).

The gradient decent method will update  $\Gamma_n^W$  by

$$\Gamma_n^W - t \frac{\partial J}{\partial \Gamma_n^W},$$

where  $t > 0$  represents the step-size. Since the step-size is fixed for each iteration in BP, assume  $t = 1$ . Let  $\omega_{mn}^{(0)} = \frac{\eta g_{mn}(\Gamma) e^{-\Gamma_n^W}}{1 + e^{-\Gamma_n^W}}$  and  $\omega_{mn}^{(1)} = \frac{\eta g_{mn}(\Gamma) e^{-\Gamma_n^W}}{e^{-\Gamma_n^X} + e^{-\Gamma_n^Y} + e^{-\Gamma_n^Z} - e^{-\Gamma_n^{S_{mn}}}}$ .

Since  $\eta g_{mn}(\Gamma) > 0$ , both  $\omega_{mn}^{(0)}$  and  $\omega_{mn}^{(1)}$  are positive. Then we have  $\Gamma_n^W$  updated by

$$\Lambda_n^W - \sum_{\substack{m \in \mathcal{M}(n) \\ S_{mn}=W}} \omega_{mn}^{(0)} \tilde{\Delta}_{m \rightarrow n} + \sum_{\substack{m \in \mathcal{M}(n) \\ \langle W, S_{mn} \rangle = 1}} \omega_{mn}^{(1)} \tilde{\Delta}_{m \rightarrow n}. \quad (12)$$

Consequently the update direction depends on the sign of  $\tilde{\Delta}_{m \rightarrow n}$ .

Comparing Eqs. (12) and (14) (with  $\alpha = 1$  and  $\beta = 0$  for conventional BP), one finds that the conventional BP decoding algorithm bears a similarity with the gradient optimization process, but has a more elegant step update direction; in our simulations, the performance of BP is better using  $\Delta_{m \rightarrow n}$  than  $\tilde{\Delta}_{m \rightarrow n}$ . The reason is that the strength of  $\Delta_{m \rightarrow n}$ , which has been resized by  $\tanh^{-1}$ , matches the marginal distribution of each qubit, conditioned on a given syndrome vector, as derived in [27].

Before we develop our MBP<sub>4</sub> in Sec. IIID, let us first analyze the difficulties that BP suffers in decoding quantum codes with high degeneracy.

### C. Energy topology

One may also consider the energy function  $J$  in Eq. (7) as a sum of the convex distance and the non-convex parity-check satisfaction terms. Since the non-convex term is the more difficult part in optimization, for simplicity, we analyze the energy topology with only the parity-check satisfaction term  $J_S(\Gamma)$ .

Figure 2 illustrates the energy topographies of a classical and a quantum decoding problems. In Fig. 2(a),

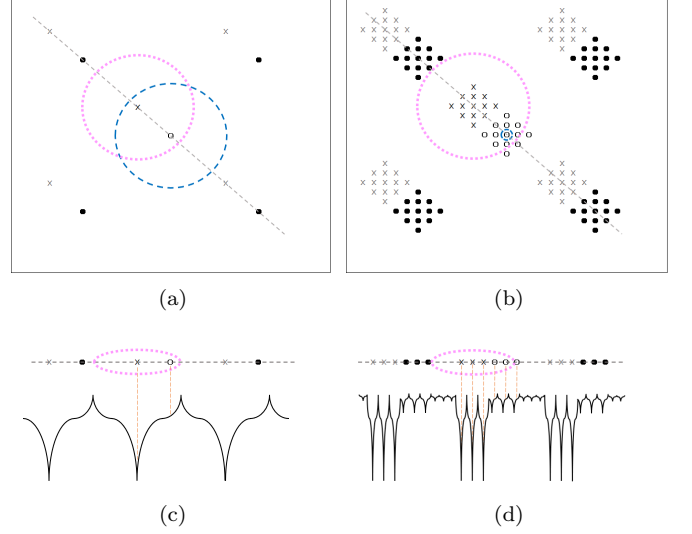


FIG. 2. Illustrations of the energy topology  $J_S$  of the decoding problem. (a) A classical code. (b) A degenerate quantum code. (c) and (d) are the profiles of the topologies along a dashed line in (a) and (b), respectively.

the small circle in the center denotes the all-zero vector, which will be called the *origin* of the topography. The other black solid circles denote certain low-weight code-words. The (blue) dashed circle is a classical *Hamming ball* with a diameter  $d$  centered at the origin. The target error is denoted by a cross in the (blue) Hamming ball. The other crosses have the same error syndrome as the target error. We also draw a (purple) dotted cycle with diameter  $d$  centered at the target error. There will be energy barriers around this cycle's boundary as shown in Fig. 2(c), which is the energy profile along the diagonal dashed line in Fig. 2(a). A syndrome-based BP starts from a point near the origin and its goal is to find the target error, which corresponds to a global minimum of the energy function. In our case, the starting point lies in a local convex hull of the target error. Since BP is like a gradient decent optimization as shown in the previous subsection, the target error can be found by BP. Sometimes, the shape of a local minimum is very narrow and BP may converge better using a smaller step-size. This is usually done by message normalization [67, 68].

For nondegenerate quantum codes, their decoding behaviors are like classical codes and BP usually works well with the techniques of message normalization and message scheduling (see examples in [25, 26]). However, BP fails to decode highly-degenerate quantum codes [33–35], such as the surface codes [8, 9]. Next we will analyze the energy topology of a degenerate quantum code.

Figure 2(b) illustrates the energy topology of a degenerate quantum code. The small circles in the center denotes the low-weight stabilizers. Each group of black solid circles denote a coset that is a set of equivalent logical operators in  $N(\mathcal{S}) \setminus \mathcal{S}$ . This is because the quantum

code is degenerate, and there are low-weight stabilizers closer to  $I^{\otimes N}$  than the other operators in  $N(\mathcal{S}) \setminus \mathcal{S}$ . The target error and its low-weight degenerate errors are the crosses in the (purple) dotted circle. The other groups of crosses are logical errors with the same error syndrome as the target error. Similarly, a syndrome-based BP starts from a point near the origin ( $I^{\otimes N}$ ). The energy profile along the diagonal dashed line in Fig. 2 (b) is shown in Fig. 2 (d). Because of the low-weight stabilizers, there are many ripples in the shape of the topology, causing conventional BP to get stuck or wander around this region. Note that mathematically the function  $J_S$  has several singular points corresponding to operators that match the given syndrome. However, BP will not get to these singular points since the values of the LLRs are numerically protected in simulation.

To help BP out of these local traps, one should use, instead, a large enough step-size to escape, unlike the classical case where a small step-size is preferred for convergence. On the other hand, due to the degeneracy of the quantum code, there are many equivalent solutions for BP and it suffices to find a degenerate error of the target. Exploiting this degeneracy may improve the performance of BP. Using a large step-size may help BP to approach any of the degenerate errors. However, using only larger steps in BP may deteriorate the convergence behavior. In the next subsection we will show that this issue can be mitigated by introducing a mechanism of *inhibition*.

#### D. BP with additional memory effect (MBP)

Motivated from the analysis of the energy topology of a degenerate quantum code and the gradient decent optimization process in the previous subsections, we propose the quaternary quantum BP in log domain with additional memory effect (abbreviated MBP<sub>4</sub>) in Algorithm 1. Our update rule for  $\Gamma_n$  in Eq. (14) parallels to Eq. (12), suggested by the gradient of the energy topology. We use two unifying parameters  $\alpha^{-1}, \beta \in \mathbb{R}$  for all the check nodes for simplicity. One may introduce additional parameters  $\alpha_{mn}$  and  $\beta_{mn}$  for each edge  $(m, n)$ , but this would require us to develop a strategy of choosing these parameters.

Algorithm 1 is presented in a different way from that in [27] with check-to-variable message  $\Delta_{m \rightarrow n}$  and variable-to-check message  $\lambda_{S_{mn}}(\Gamma_{n \rightarrow m})$ . Especially Eq. (15) can be written as

$$\Gamma_{n \rightarrow m}^W = \Lambda_n^W + \frac{1}{\alpha} \sum_{\substack{m' \in \mathcal{M}(n) \\ \langle W, S_{m'n} \rangle = 1}} \Delta_{m' \rightarrow n} - \beta \sum_{\substack{m' \in \mathcal{M}(n) \\ S_{m'n} = W}} \Delta_{m' \rightarrow n} - \langle W, S_{mn} \rangle \Delta_{m \rightarrow n}. \quad (16)$$

The term  $-\langle W, S_{mn} \rangle \Delta_{m \rightarrow n}$  is called *inhibition*, which provides adequate strength to resist a wrong belief looping in the short cycle. Unlike [25, 27], where the corresponding inhibition is also scaled by  $1/\alpha$ , we suggest to

---

#### Algorithm 1 : Quaternary BP with additional memory effect (MBP<sub>4</sub>)

---

**Input:**  $S \in \{I, X, Y, Z\}^{M \times N}$ ,  $z \in \{0, 1\}^M$ ,  $T_{\max} \in \mathbb{Z}_+$ , real  $\alpha, \beta > 0$ , and initial LLR vectors  $\{(\Lambda_n^X, \Lambda_n^Y, \Lambda_n^Z) \in \mathbb{R}^3\}_{n=1}^N$ .  
**Initialization.** For  $n = 1, 2, \dots, N$ ,  $W \in \{X, Y, Z\}$ , and  $m \in \mathcal{M}(n)$ , let

$$\Gamma_{n \rightarrow m}^W = \Lambda_n^W.$$

**Horizontal Step.** For  $m = 1, 2, \dots, M$  and  $n \in \mathcal{N}(m)$ , compute

$$\Delta_{m \rightarrow n} = (-1)^{z_m} \bigoplus_{n' \in \mathcal{N}(m) \setminus \{n\}} \lambda_{S_{mn'}}(\Gamma_{n' \rightarrow m}). \quad (13)$$

**Vertical Step.** For  $n = 1, 2, \dots, N$  and  $W \in \{X, Y, Z\}$ , compute

$$\Gamma_n^W = \Lambda_n^W + \frac{1}{\alpha} \sum_{\substack{m \in \mathcal{M}(n) \\ \langle W, S_{mn} \rangle = 1}} \Delta_{m \rightarrow n} - \beta \sum_{\substack{m \in \mathcal{M}(n) \\ S_{mn} = W}} \Delta_{m \rightarrow n}. \quad (14)$$

- **(Hard Decision.)** Let  $\hat{E} = \hat{E}_1 \hat{E}_2 \dots \hat{E}_N$ , where  $\hat{E}_n = I$  if  $\Gamma_n^W > 0$  for all  $W \in \{X, Y, Z\}$ , and  $\hat{E}_n = \arg \min_{W \in \{X, Y, Z\}} \Gamma_n^W$ , otherwise.
- If  $\langle \hat{E}, S_m \rangle = z_m \forall m$ , halt and return “CONVERGE”;
- Otherwise, if the maximum number of iterations  $T_{\max}$  is reached, halt and return “FAIL”;
- **(Fixed Inhibition.)** Otherwise, for  $n = 1, 2, \dots, N$ ,  $W \in \{X, Y, Z\}$ , and  $m \in \mathcal{M}(n)$ , compute

$$\Gamma_{n \rightarrow m}^W = \Gamma_n^W - \langle W, S_{mn} \rangle \Delta_{m \rightarrow n}. \quad (15)$$

- Repeat from the horizontal step.
- 

keep this inhibition strength (Eq. (16)) since this part is the belief inherited in check node  $m$ , and it must remain unchanged when we update the belief in variable  $n$  to make the decoding less affected by the short cycles.

How to choose the factor  $\alpha$  is intriguing. The gradient optimization step suggests that  $\alpha \propto 1/g_{mn}(\Gamma)$  by Eq. (9). Since  $\Gamma$  is initialized as the channel statistics vector  $\Lambda$  at the first step and  $\alpha$  is fixed in BP for simplicity, we plot  $1/g_{mn}(\Lambda)$  as a function of the channel depolarizing rate  $\epsilon$  in Fig. 3 for various stabilizer weight  $k = |\mathcal{N}(m)|$ . Basically,  $1/g_{mn}(\Lambda)$  is larger as  $\epsilon$  gets smaller. In addition,  $1/g_{mn}(\Lambda)$  is larger for stabilizers of larger weight. This is consistent with our simulation results in Fig. 17 in Appendix B. However, for investigation, we will simulate as many values of  $\alpha$  as possible. In fact, the magnitude of  $g_{mn}$  is very small and for a gradient decent with constant step-size  $t = 1$ , we need to use the factor  $\eta$  to adjust the energy function and consequently the step-size. This will be discussed more in Appendix C.

Next we discuss the term  $-\beta \sum_{\substack{m' \in \mathcal{M}(n) \\ S_{m'n} = W}} \Delta_{m' \rightarrow n}$  in Eq. (16), which is also like an inhibition. Since it is in-



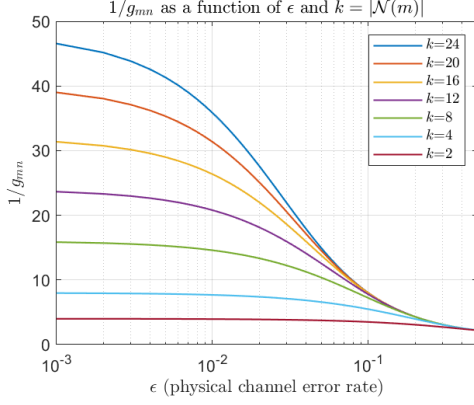


FIG. 3. Plot of  $1/g_{mn}(\Lambda)$  as a function of  $\epsilon$  and various  $k = |\mathcal{N}(m)|$ .

duced from gradient decent optimization, we simply have a step-size  $\beta$  to adjust its strength. However, we find that in most cases, MBP<sub>4</sub> performs better with  $\beta = 0$ ; for the five-qubit code, MBP<sub>4</sub> performs better with large  $\beta$  for large depolarizing rate  $\epsilon$  (this will be discussed later in Sec. IV A).

**Remark 2** When  $\beta = 0$ , one can verify that

$$\lambda_{S_{mn}}(\Gamma_{n \rightarrow m}) = \lambda_{S_{mn}}(\Gamma_n) - \Delta_{m \rightarrow n}. \quad (17)$$

It is more efficient to update  $\lambda_{S_{mn}}(\Gamma_{n \rightarrow m})$  in this way since for each  $n$ ,  $\lambda_{S_{mn}}(\Gamma_n)$  needs to be computed at most three computations of  $\lambda_{S_{mn}}(\cdot)$  for  $S_{mn} \in \{X, Y, Z\}$ ; on the other hand, directly computing  $\lambda_{S_{mn}}(\Gamma_{n \rightarrow m})$  needs  $|\mathcal{M}(n)|$  (usually  $\geq 3$ ) computations of  $\lambda_{S_{mn}}(\cdot)$ .

The computation in the horizontal step can be simplified as in Remarks 1 and 4 of [27]. Then the MBP<sub>4</sub> complexity is proportional to the number of edges  $Nj$  per iteration, and thus the overall complexity is  $O(Nj\tau)$ .

For reference, we provides the MBP<sub>4</sub> in linear domain (with  $\beta = 0$ ) as Algorithm 3 in Appendix A to be compared with [25, Algorithm 3].

### E. MBP Decoding as an RNN

It was known that a BP decoding process can be modeled as an RNN [38, 49]. Similarly we can derive an RNN from Algorithm 1 (with  $\beta = 0$  for simplicity). The RNN usually represent the BP with a parallel schedule. In the Tanner graph corresponding to the  $M \times N$  check matrix  $S$ , two types of messages are iteratively updated: variable-to-check and check-to-variable messages. Hence, there will be two hidden neuron layers computing messages  $\Delta_{m \rightarrow n}$  or  $\lambda_{S_{mn}}(\Gamma_{n \rightarrow m})$  per edge alternatively in each layer, and there are  $N$  input neurons  $\{\Lambda_n\}_{n=1}^N$  and  $N$  output neurons  $\{\Gamma_n\}_{n=1}^N$ . An estimated error  $\hat{E}$  will be inferred from  $\{\Gamma_n\}_{n=1}^N$ . The RNN will iterate until a

valid  $\hat{E}$  with syndrome  $z$  is found or a maximum number of iterations  $T_{\max}$  is reached.

Figure 4(a) illustrates the RNN derived from the BP on the Tanner graph in Fig. 1. The neurons denoted by  $\Gamma_{n \rightarrow m}$  will compute messages  $\lambda_{S_{mn}}(\Gamma_{n \rightarrow m})$  but this is not explicitly shown. Note that there are additional edges (dotted curves) from  $\Delta_{m \rightarrow n}$  to  $\lambda_{S_{mn}}(\Gamma_{n \rightarrow m})$ , which are not considered in the previous BP methods [11, 25, 32–34], nor in the neural networks of the neural BP [38, 49].

These edges provide a memory effect as discussed in the remark following Eq. (16), which contributes to the major improvement. This agrees to the known result that using proper inhibition between neurons enhances a network's perception capability in Hopfield nets [43–47].

Figure 4(b) shows another (equivalent) way of updating  $\Gamma_{n \rightarrow m}$  by Eq. (15). If we simply consider conventional BP, then every solid edge in Fig. 4(a) is an excitation (with positive weight  $+1$  in BP); in Fig. 4(b), every dashed line is an excitation, but a solid line is an inhibition (with negative weight  $-1$  in BP).

To sum up, we have shown that MBP<sub>4</sub> can be extended to a neural network decoder, which may be further improved by using appropriate weight  $\alpha$  for each edge.

### F. Adaptive MBP

In this subsection, we propose a variation of MBP with  $\alpha$  chosen adaptively as shown in Algorithm 2. The value of  $\alpha$  controls the search radius of MBP<sub>4</sub>. Typically, a fixed  $\alpha$  is chosen so that BP focuses on an error correction region, e.g.,  $1 \times \text{BDD}$  to  $2 \times \text{BDD}$ . For codes with high degeneracy, we intend to correct errors of higher weight and consequently we need to consider variations in  $\alpha$ . Moreover,  $\alpha$  should be chosen according to each syndrome vector and the channel statistics.

Precisely selecting a proper  $\alpha$  helps to achieve a desired performance but in general it is difficult to do so. Generating a solution by referring multiple instances of the decoder is an important technique in Monte Carlo sampling methods (cf. parallel tempering in [48]) and in neural networks (cf. [49, Fig. 4]). This is like an  $\epsilon$ -net. Thus we conduct multiple instances of MBP<sub>4</sub> (which can be done in parallel or serial order) each with a different value of  $\alpha$ , and choose the valid (syndrome-matched) solution output with the largest (the most conservative)  $\alpha$ . This value of  $\alpha$  will be denoted by  $\alpha^*$  and MBP<sub>4</sub> with  $\alpha^*$  chosen by Algorithm 2 will be denoted by MBP<sub>4</sub>( $\alpha^*$ ).

Note that the procedure in Algorithm 2 tests each value of  $\alpha_i$  in a sequential manner; these  $\alpha_i$ 's can be tested in parallel if the physical resources for implementation are available, followed by a final check.



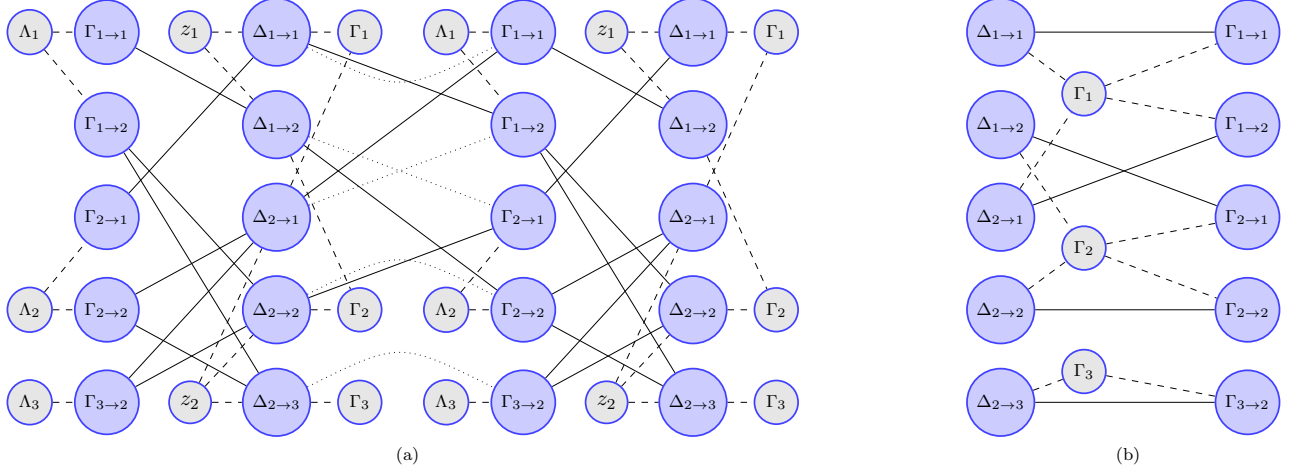


FIG. 4. (a) An RNN converted from Fig. 1 with the first two iterations unrolled according to Eqs. (13) and (16). Since there are five edges in Fig. 1, the RNN has five neurons per hidden layer. (b) Another (equivalent) way to update  $\lambda_{S_{mn}}(\Gamma_{n \rightarrow m})$  between the two iterations in (a) according to Eq. (15) (or Eq. (17)). In both figures, small circles are input/output neurons, and large circles are hidden neurons. A solid line is an edge connecting hidden neurons  $\Gamma_{n \rightarrow m}$  and  $\Delta_{m \rightarrow n}$ . A dashed line is an edge connecting a hidden neuron and an input/output neuron. A dotted line in (a) is a special edge with gain  $-(1 - \frac{1}{\alpha})$  so that  $\Delta_{m \rightarrow n}$  is rescaled and added to  $\Gamma_{n \rightarrow m}^W$  when  $\langle W, S_{mn} \rangle = 1$  as in Eq. (16). This edge is implicitly embedded in (b) by Eq. (15).

---

**Algorithm 2** : Adaptive MBP<sub>4</sub> (to find  $\alpha^*$  by incremental step-size  $1/\alpha_i$ )

---

**Input:**  $S \in \{I, X, Y, Z\}^{M \times N}$ ,  $z \in \{0, 1\}^M$ ,  $T_{\max} \in \mathbb{Z}_+$ ,  $\{\Lambda_n = (\Lambda_n^X, \Lambda_n^Y, \Lambda_n^Z) \in \mathbb{R}^3\}_{n=1}^N$ , a sequence of real values  $\alpha_1 > \alpha_2 > \dots > \alpha_l > 0$ , and an oracle function MBP<sub>4</sub>.

**Initialization:** Let  $i = 1$  and  $\beta = 0$ .

**MBP Step:** Run MBP<sub>4</sub>( $S, z, T_{\max}, \alpha_i, \beta, \{\Lambda_n\}$ ),

which will return “CONVERGE” or “FAIL” with estimated  $\hat{E} \in \{I, X, Y, Z\}^N$ .

**Adaptive Check:** Let  $i \leftarrow i + 1$ .

- If the return indicator is “CONVERGE”, return “SUCCESS” (with valid  $\hat{E}$  and  $\alpha^* = \alpha_i$ );
  - If  $i > l$ , return “FAIL” (with invalid  $\hat{E}$ );
  - Otherwise, repeat from the MBP Step.
- 

#### IV. SIMULATIONS OF VARIOUS QUANTUM CODES

In this section, we first study Algorithm 1 on the well-known  $[[5, 1, 3]]$  code [53]. Then we simulate the decoding performance of MBP<sub>4</sub> with  $\beta = 0$  and various values of  $\alpha$  on quantum bicycle codes, a generalized hypergraph-product code, and surface codes.

When evaluating the logical error rate or other error rates, an error bar between two crosses shows a 95% confidence interval if fewer than 100 error events are collected.

In the following discussion, we will discard the global phase; or equivalently, when we refer  $\mathcal{S}$ , it includes  $\pm \mathcal{S}$ .

In simulations, a decoding is successful if it outputs an estimated error  $\hat{E} \in ES$ . Thus it is important to determine whether an estimated error  $\hat{E}$  is a degenerate error of the target error  $E$ . For convenience, some literature may consider a decoding successful only when  $\hat{E} = E$  [69]; however, this is not accurate, especially for highly-degenerate codes. A simple observation here is that  $\hat{E} \in ES$  if and only if  $\hat{E}E \in \mathcal{S}$ .

**Lemma 3** Suppose that  $\{\bar{X}_1, \bar{Z}_1, \dots, \bar{X}_K, \bar{Z}_K\}$  is an independent generating set for  $N(\mathcal{S}) \setminus \mathcal{S}$ . Then  $\hat{E} \in ES$  if and only if  $\hat{E}E$  commutes with  $S_m$ ’s,  $\bar{X}_k$ ’s and  $\bar{Z}_k$ ’s.

An efficient method to find  $\bar{X}_k$ ’s and  $\bar{Z}_k$ ’s is by using the standard form provided in [6].

Next we discuss how degeneracy is exploited. Let  $n_{\text{tot}}$  be the number of tested error samples for a data point in simulations. Suppose that  $E^{(i)}$  and  $\hat{E}^{(i)}$  are tested and estimated errors, respectively, for  $i = 1, 2, \dots, n_{\text{tot}}$ . Let

$$n_0 = \# \text{ of pairs } (E^{(i)}, \hat{E}^{(i)}) : \hat{E}^{(i)} \neq E^{(i)}, \quad (18)$$

$$n_e = \# \text{ of pairs } (E^{(i)}, \hat{E}^{(i)}) : \hat{E}^{(i)} \notin E^{(i)}\mathcal{S}, \quad (19)$$

$$n_u = \# \text{ of pairs } (E^{(i)}, \hat{E}^{(i)}) : \hat{E}^{(i)}E^{(i)} \in N(\mathcal{S}) \setminus \mathcal{S}. \quad (20)$$

Empirically, we have the *classical block error rate*  $P(\hat{E} \neq E) = n_0/n_{\text{tot}}$ , the *quantum logical error rate*  $P(\hat{E} \notin ES) = n_e/n_{\text{tot}}$ , and the *undetected error rate*  $P(\hat{E}E \in N(\mathcal{S}) \setminus \mathcal{S}) = n_u/n_{\text{tot}}$ .

Since  $(\hat{E} \notin ES) \subseteq (\hat{E} \neq E)$ , by Bayes rule, we have

$$\begin{aligned} P(\hat{E} \notin ES) &= P(\hat{E} \notin ES, \hat{E} \neq E) \\ &= P(\hat{E} \neq E) \times P(\hat{E} \notin ES \mid \hat{E} \neq E) = \frac{n_0}{n_{\text{tot}}} \times \frac{n_e}{n_0}. \end{aligned} \quad (21)$$

Usually a classical strategy to improve decoding is trying to lower  $n_0/n$ , which means that a target error needs to be accurately located from a given syndrome. Such a strategy has a limit in performance due to short cycles or strong code degeneracy. A better strategy should also try to improve  $n_e/n_0$ , which will be called the error suppression ratio from exploiting the degeneracy. For example, if the decoder converges to any of the degenerate errors, the decoding is a success (i.e.,  $n_0$  may +1 but  $n_e$  not).

Recall that Algorithm 1 with  $\alpha = 1$  and  $\beta = 0$  is equivalent to the conventional quaternary BP (conventional  $BP_4$ , or in short,  $BP_4$ ). We will demonstrate that  $MBP_4$  outperforms  $BP_4$  on various kinds of quantum codes.

For comparison, we will also consider  $BP_4$  with typical message normalization (denoted by  $\alpha_c$ ), as follows [27], which is like classical message normalization [67, 68]. Given some  $\alpha_c > 0$ , in Algorithm 1,

$$\begin{aligned}\Gamma_{n \rightarrow m}^W &= \Lambda_n^W + \frac{1}{\alpha_c} \sum_{\substack{m' \in \mathcal{M}(n) \\ \langle W, S_{m'n} \rangle = 1}} \Delta_{m' \rightarrow n} - \frac{1}{\alpha_c} \langle W, S_{mn} \rangle \Delta_{m \rightarrow n} \\ &= \Lambda_n^W + \frac{1}{\alpha_c} \sum_{\substack{m' \in \mathcal{M}(n) \setminus m \\ \langle W, S_{m'n} \rangle = 1}} \Delta_{m' \rightarrow n},\end{aligned}\quad (22)$$

and this decoding will be referred to as *normalized  $BP_4$* .

BP can run with the parallel or serial schedule. (For the conversion of the schedules, see [25].) Algorithm 1 using each of these schedules will be referred to as *parallel  $MBP_4$*  or *serial  $MBP_4$* . Similarly, we have *parallel  $BP_4$*  or *serial  $BP_4$*  for conventional BP, and *parallel  $MBP_4(\alpha^*)$*  or *serial  $MBP_4(\alpha^*)$*  if  $\alpha^*$  is chosen by Algorithm 2. We may also consider *parallel normalized  $BP_4$*  or *serial normalized  $BP_4$* . If a BP algorithm is referred without the prefix *parallel* or *serial*, the parallel schedule is assumed.

### A. The $[[5,1,3]]$ code

The  $[[5,1,3]]$  code [53] has a check matrix

$$S = \begin{bmatrix} X & Z & Z & X & I \\ I & X & Z & Z & X \\ X & I & X & Z & Z \\ Z & X & I & X & Z \end{bmatrix}.$$

This code is worth investigation because there are many four-cycles in a small check matrix. We remark that using the serial schedule enables conventional  $BP_4$  to decode the  $[[5,1,3]]$  code [25]. Herein we use  $MBP_4$  with the parallel schedule (parallel  $MBP_4$ ) to investigate the effect of  $\alpha$  and  $\beta$ .

We simulate Algorithm 1 with various  $\alpha$  at  $\beta = 0$  to decode the  $[[5,1,3]]$  code. The performance curves for  $\epsilon < 0.1$  are plotted in Fig. 5, where the BDD performance curve is also provided.  $MBP_4$  with  $\alpha \approx 1.5$  has the best performance and it competes with BDD for  $\epsilon < 0.005$ . Next we simulate Algorithm 1 with various  $\beta$  at  $\alpha = 1.5$  and the results are shown in Fig. 6. It suggests to choose  $\beta = 0$  for  $\epsilon < 10^{-3}$  and  $\beta \approx 1$  for  $\epsilon > 10^{-2}$ . This is

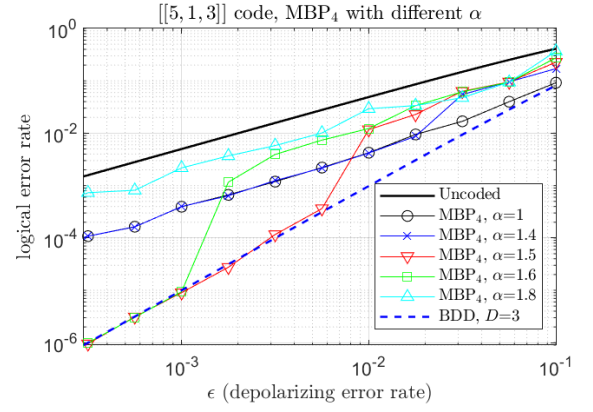


FIG. 5. Decoding the  $[[5,1,3]]$  code using parallel  $MBP_4$  with various  $\alpha$  at  $\beta = 0$ .

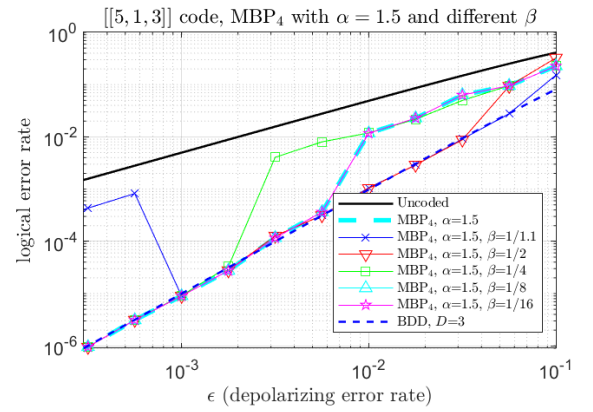


FIG. 6. Decoding the  $[[5,1,3]]$  code using parallel  $MBP_4$  with various  $\beta$  at  $\alpha = 1.5$ .

reasonable since, for large  $\epsilon$ , initial  $\Gamma_n^W = \Lambda_n^W$  is small, and thus  $\beta \propto \frac{\eta g_{mn}(\Gamma) e^{-\Gamma_n^W}}{1 + e^{-\Gamma_n^W}}$  is large according to Eq. (9).

The  $[[5,1,3]]$  code can correct any single-qubit error, but conventional  $BP_4$  (the case with  $\alpha = 1$ ) fails to decode the error  $IIII$ , no matter what value  $\beta$  is.

In the following, we simply consider  $\beta = 0$ . We plot  $\Gamma_n$  at each iteration in decoding  $IIII$  at  $\epsilon = 0.003$  in Fig. 7, where  $\Gamma_n = \Lambda_n$  at iteration 0. With  $\alpha = 1$ , the state of  $\Gamma_n$  oscillates between  $IIII$  and  $YYYY$  continuously. If  $\alpha = 1.5$  is used instead,  $MBP_4$  has a resistance to the wrong belief, and the decoding converges correctly.

We plot the change of  $J_S$  in Fig. 8. Figures 8(a) and 8(b) correspond to Figs. 7(a) and 7(b), respectively. With  $\alpha = 1$ , the value of  $J_S$  oscillates around 21.3 with a small swing. Using  $\alpha = 1.5$ ,  $MBP_4$  enlarges the swing and  $J_S$  finally goes to a small value less than zero.

We also provide the result of normalized  $BP_4$  with  $\alpha_c = 1.5$  as in Eq. (22). In this case,  $J_S$  oscillates between roughly 8 and 19 continuously.

Next we consider BP decoding with a fixed  $\epsilon_0 = 0.003$  to initialize  $\Lambda_n$ , regardless of the actual depolarizing rate. We find that the performance curve of  $MBP_4$  with  $\alpha =$

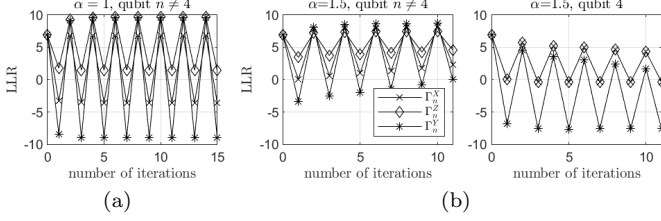


FIG. 7. The change of the state  $\Gamma_n = (\Gamma_n^X, \Gamma_n^Y, \Gamma_n^Z)$  in decoding the  $[[5, 1, 3]]$  code with error  $IIIYI$  at  $\epsilon = 0.003$ . (a)  $MBP_4$  with  $\alpha = 1$  (conventional  $BP_4$ ) for qubit  $n \neq 4$ . The case of  $n = 4$  is similar but with a different amplitude. (b)  $MBP_4$  with  $\alpha = 1.5$ .

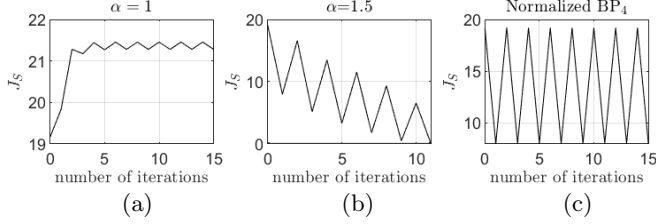


FIG. 8. The evolution of  $J_S$  (Eq. (8)) for decoding the  $[[5, 1, 3]]$  code with error  $IIIYI$  at  $\epsilon = 0.003$ . (a)  $MBP_4$  with  $\alpha = 1$ . (b)  $MBP_4$  with  $\alpha = 1.5$ . (c) Normalized  $BP_4$  with  $\alpha_c = 1.5$ .

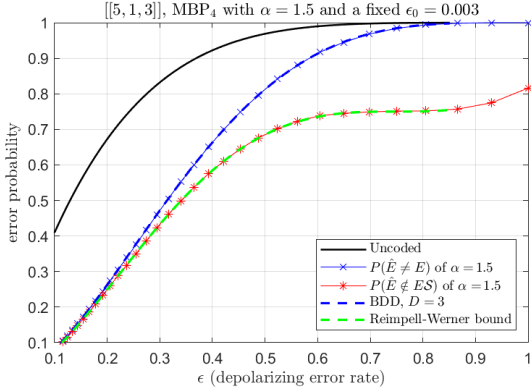


FIG. 9. Decoding the  $[[5, 1, 3]]$  code using parallel  $MBP_4$  with  $\alpha = 1.5$  and a fixed  $\epsilon_0 = 0.003$  to initialize  $\Lambda_n$ .  $P(\hat{E} \neq E)$  is the classical block error rate, which is comparable with BDD.  $P(\hat{E} \notin ES)$  is the quantum logical error rate, which matches the Reimpell-Werner bound.

1.5 matches the BDD curve for  $\epsilon < 0.1$ . Even more, it achieves the Reimpell-Werner bound for the  $[[5, 1, 3]]$  code [70], which outperforms the BDD at a large  $\epsilon$  due to the degeneracy. The curves of BDD, Reimpell-Werner bound, and  $MBP_4$  with  $\alpha = 1.5$  are compared in Fig. 9.

**Remark 4** Initializing  $\Lambda$  with respect to a fixed  $\epsilon_0$ , instead of the actual depolarizing rate, is a strategy to maintain the decoding stability without curve fluctuation in practice [50] [71]. This also reflects the importance of choosing the network initial state [51]. This technique of

fixed initialization works for any quantum codes, especially when the channel parameter is hard to estimate.

We keep  $\beta = 0$  in the following.

## B. Bicycle code

Bicycle codes are a kind of random sparse-graph code with designed code rate and row-weight, and their performance could be close to the quantum Gilbert–Varshamov bound [11]. Let  $k$  be the row-weight of a bicycle code. A smaller  $k$  means the code has many low-weight stabilizers and the code is more degenerate. However, since the minimum distance of the code  $\leq k$  due to the construction [11], if  $k$  is too-small, it may have a high error-floor.

MacKay *et al.* showed that, for a bicycle code with  $[[N, K]] = [[3786, 946]]$ , a row-weight  $k \geq 24$  is required to have good BP performance at a target block error rate  $10^{-4}$  [11, Fig. 6]. We construct bicycle codes with the same parameters. Figure 10(a) shows the conventional  $BP_4$  performance on  $[[3786, 946]]$  bicycle codes with  $k = 24, 20, 16, 12$ . It agrees with [11, Fig. 6] that a larger row-weight  $k = 24$  is required to achieve the logical error rate of  $10^{-4}$  before hitting the error-floor. Also shown in Fig. 10(a) are the binary BP ( $BP_2$ ) performance curves in [11]. It can be seen that  $BP_4$  performs better than  $BP_2$ , because the correlations between  $X$  errors and  $Z$  errors are considered in  $BP_4$  (cf. [11, Fig. 11]).

Now we use  $MBP_4$  with  $\alpha > 1$ , and the performance is significantly improved, as shown in Fig. 10(b). (Note that we use different  $\alpha$  for different  $\epsilon$  as shown in Appendix B.) It shows that a bicycle code of row-weight  $k = 16$  is able to achieve the logical error rate of  $10^{-6}$ , which is less affected by the error-floor. Thus we have greatly improved the BP performance on bicycle codes.

The minimum distance  $D$  of a bicycle code is unknown, so it is hard to compare with  $r \times BDD$  as in Definition 1. However,  $D \leq k$  as mentioned above. Instead, we directly specify the correction radius  $t$  and plot some BDD curves in Fig. 10(b). For  $k = 16$ , depending on the logical error rate, the performance of  $MBP_4$  is close to BDD with  $t$  between 140 and 200, despite the fact that  $D \leq 16$ , far more smaller than 140 or 200. Note that, as  $D/2 \leq 8$ , if  $t = 170$  is considered, it is more than  $20 \times BDD$ .

Although it is not shown,  $MBP_4$  outperforms normalized  $BP_4$ , especially for small  $k$ . Note that a comparison of the neural BP [38] and normalized  $BP_4$  on  $[[256, 32]]$  bicycle codes was given in [27]; it would be difficult to use neural BP on large code sizes such as  $[[3786, 946]]$  here.

The average numbers of iterations are shown in Fig. 10(c). After applying  $\alpha$ , the iterations can be reduced if the decoder has better convergence behavior. For  $k = 12$ , the convergence improvement is obvious since there are more lower-weight stabilizers and hence more low-weight degenerate errors.

Next we study whether  $MBP_4$  improves the error suppression ratio  $n_e/n_0$  considered in Eq. (21). We remark

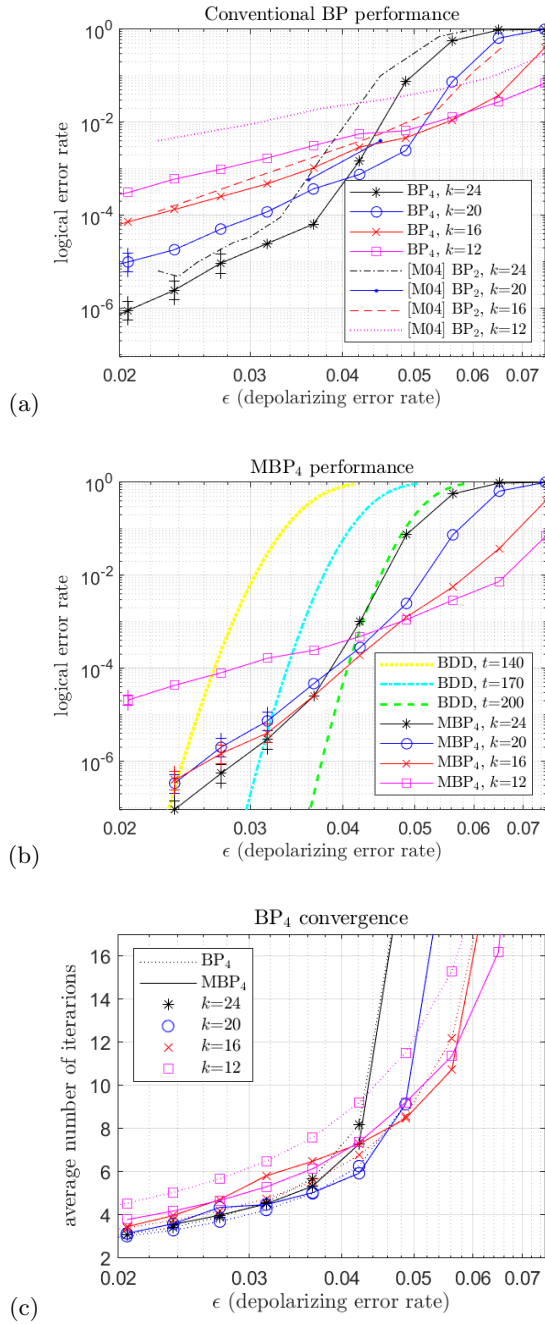


FIG. 10. Performance of parallel BP<sub>4</sub> and MBP<sub>4</sub> on the  $[[3786, 946]]$  bicycle codes with different row-weights  $k$ , based on  $T_{\max} = 90$ . (a) MBP<sub>4</sub> with  $\alpha = 1$  (conventional BP<sub>4</sub>). (b) MBP<sub>4</sub> with appropriate  $\alpha > 1$ . (c) Average numbers of iterations in (a) (dotted lines) and (b) (solid lines). The [M04] curves in (a) are from [11, Fig. 6] (through a conversion from bit-flip error rate to depolarizing error rate [11, Eq. (40)]).

that BP<sub>4</sub> in Fig. 10 (a) has  $n_e/n_0 \approx 1$  for all cases. MBP<sub>4</sub> in Fig. 10 (b) starts to have  $n_e/n_0 < 1$  for  $k \leq 16$ . We list some raw data of Fig. 10 (b) in Table II. It shows that MBP<sub>4</sub> has a smaller  $n_e/n_0$  for a smaller  $k$ , i.e., the decoder exploits the degeneracy more for a code with lower-weight stabilizers. Fixing to  $k = 16$  or 12, for a

TABLE II. Numbers of various events for the simulations in Fig. 10 (b) with  $\alpha > 1$ .  $n$  is the number of tested codewords.

$\epsilon$	0.027	0.037	0.049
$k = 16 : n_{\text{tot}}$	12635150	3920434	79172
$n_0$	34	126	102
$n_e$	20	100	100
$n_u$	0	0	0
$k = 12 : n_{\text{tot}}$	1251769	410670	89821
$n_0$	518	466	270
$n_e$	100	100	100
$n_u$	1	3	2

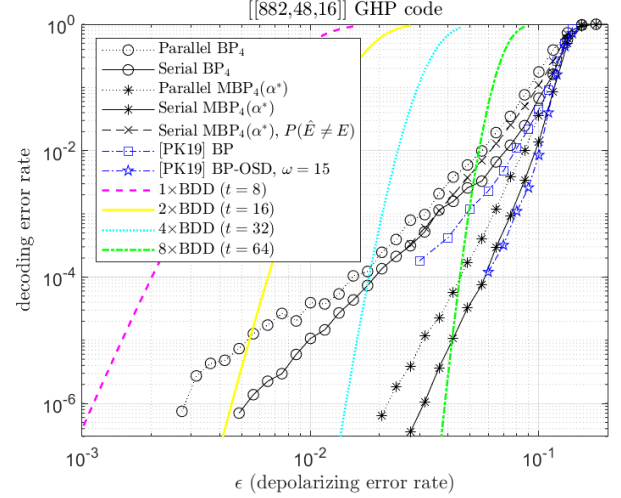


FIG. 11. The performance of the  $[[822, 48, 16]]$  GHP code, based on  $T_{\max} = 32$ . The curve  $P(\hat{E} \neq E)$  is the classical block error rate, while the other curves are the quantum logical error rate with degenerate errors considered. The curves [PK19] are from [33].

smaller  $\epsilon$ , the ratio  $n_e/n_0$  is also smaller, providing a lower error-floor. It is possible to lower  $n_e/n_0$  by using  $k < 12$ , but the case of  $k = 12$  has already compromised the minimum distance, resulting in a too-high error-floor.

Also listed in Table II is the number of undetected errors. The undetected error rate  $n_u/n_{\text{tot}} \neq 0$  for  $k = 12$ . However, this is ten times lower than the case of conventional BP<sub>4</sub> with  $\alpha = 1$ .

### C. Generalized hypergraph-product code

Herein we consider the decoding of generalized hypergraph-product (GHP) codes [13], in particular, the  $[[N, K, D]] = [[882, 48, 16]]$  GHP code constructed in [33], which has row-weight  $8 < D$  and is thus highly-degenerate. The performance of this code is shown in Fig. 11. Using conventional BP<sub>4</sub> (no matter parallel or serial schedules) does not have good enough performance. Using MBP<sub>4</sub>, we find that most errors can be decoded



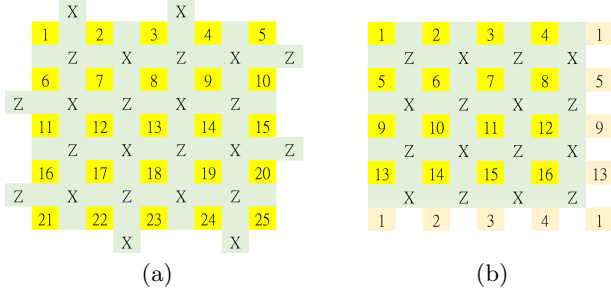


FIG. 12. (a) The lattice of the  $[[L^2, 1, L]]$  (rotated) surface code with  $L = 5$ . (b) The lattice of the  $[[L^2, 2, L]]$  (rotated) toric code with  $L = 4$ . In both figures, a qubit is represented by a yellow box numbered from 1 to  $N$ . In (b), since the toric code lie in a torus, there are orange boxes on the right and bottom, each representing the qubit of the same number. An  $X$ -type or  $Z$ -type stabilizer is indicated by a label  $W \in \{X, Z\}$  between its neighboring qubits. For example, in (a), the label  $X$  between qubits 1, 2 is  $X_1 X_2 = X \otimes X \otimes I^{\otimes(N-2)}$  and the label  $Z$  between qubits 1, 2, 6, 7 is  $Z_1 Z_2 Z_6 Z_7$ .

with  $\alpha \approx 1.2$  to 1.5. However, since this code exhibits high degeneracy, a smaller  $\alpha$  may be needed. Thus we apply Algorithm 2 with  $\{\alpha_i\}_{i=1}^l = \{1.5, 1.45, \dots, 0.5\}$  so that  $\alpha^*$  is determined for each syndrome vector.

We use  $r \times \text{BDD}$  for reference. Observe that serial  $\text{MBP}_4(\alpha^*)$  has slope roughly aligned with  $1 \times \text{BDD}$ , but its performance is close to  $8 \times \text{BDD}$  at logical error rate  $10^{-5}$ , since more low-weight errors are corrected. We also draw the curve of classical block error rate  $P(\hat{E} \neq E) = n_0/n_{\text{tot}}$ , which shows that the improvement of  $\text{MBP}_4$  mostly comes from exploiting the degeneracy.

For reference, we also plot the performance curves given in [33], where the improved one is based on BP using a layered schedule with post-processing by OSD [54] (which is powerful but has high complexity). In addition, in [33], OSD is combined with a post-selection with a parameter  $\omega$  to sort out  $2^\omega$  errors in  $\omega$  unreliable coordinates (quite high complexity). For most codes in [54], using  $\omega = 0$  is sufficient, but this GHP code needs large  $\omega = 15$  to achieve good performance.

#### D. Surface code

In this subsection we consider the surface codes with a  $45^\circ$  rotation [9]. A parallel study of rotated toric codes will be provided in Appendix B 3.

An  $[[L^2, 1, L]]$  surface code for an odd integer  $L$  can be defined on an  $L \times L$  square lattice. Figure 12 (a) shows an example of  $L = 5$ . The stabilizer generators are of weight 2 or 4 independent of  $D = L$ , so a large surface code has quite strong degeneracy.

Observe that, in Fig. 12 (a), if only the  $X$ -type stabilizer between qubits 1 and 2 has syndrome 1 but the other stabilizers have syndrome 0, then a parallel-scheduled BP is hard to distinguish which qubit, 1 or 2, has error. This

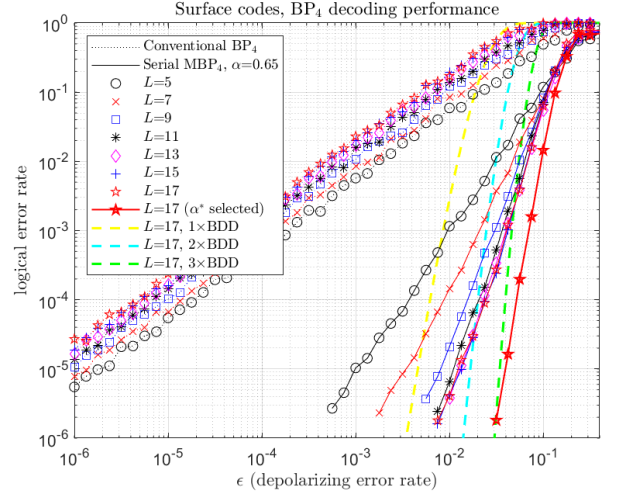


FIG. 13. Conventional  $\text{BP}_4$  and serial  $\text{MBP}_4$  decoding performance on surface codes, based on  $T_{\text{max}} = 150$ . For generating this figure, we use a fixed  $\epsilon_0 = 0.013$  to prevent the curve fluctuation (as discussed in Remark 4).

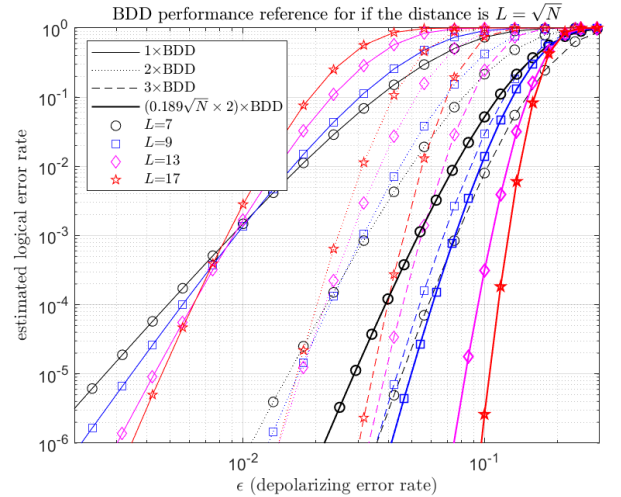


FIG. 14.  $r \times \text{BDD}$  performance curves of  $[[L^2, 1, L]]$  codes for  $r = 1, 2, 3$ , and  $0.189\sqrt{N} \times 2$ .

is like an example in the end of Sec. II B. To improve, a straightforward way is to use Algorithm 1 with the serial schedule (serial  $\text{MBP}_4$ ) and a larger step-size ( $\alpha < 1$ ).

The decoding performance of  $\text{BP}_4$  and  $\text{MBP}_4$  on surface codes is shown in Fig. 13. It can be seen that conventional  $\text{BP}_4$  does not work on surface codes; even worse, the logical error rate is higher for larger distance. The techniques of scheduling and message normalization (normalized  $\text{BP}_4$ ) are not effective either. On the other hand, using serial  $\text{MBP}_4$  with  $\alpha < 1$  significantly improves the decoding performance. Two examples of  $L = 7$  are provided in Appendix B (Fig. 18) to explain why serial  $\text{MBP}_4$  with  $\alpha < 1$  has better performances. Specifically, serial  $\text{MBP}_4$  with  $\alpha < 1$  usually finds a degenerate error,

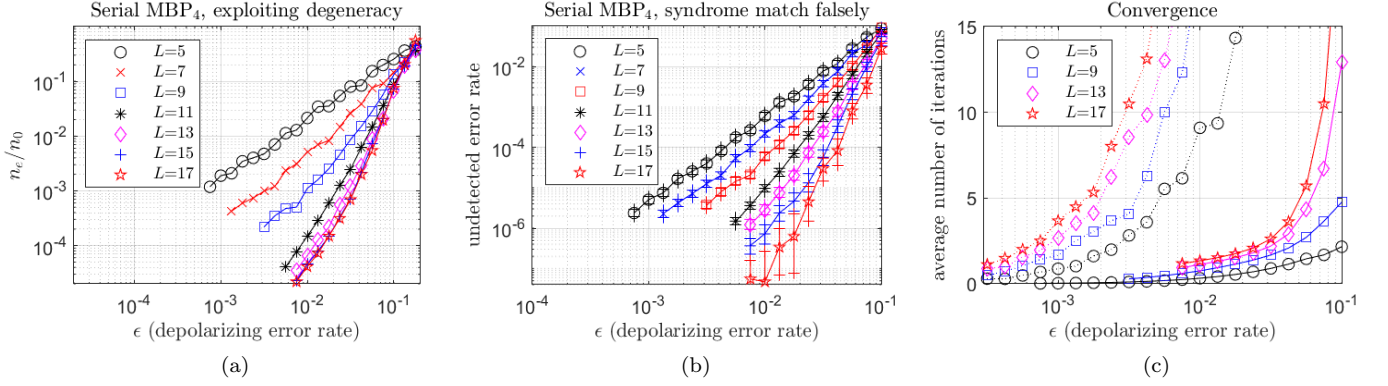


FIG. 15. Some statistics of decoding surface codes using serial  $\text{MBP}_4$  with  $\alpha = 0.65$  (solid lines). (a) The ratio  $n_e/n_0$ . (b) Undetected error rate. (c) Average numbers of iterations; also shown in (c) are the numbers for conventional  $\text{BP}_4$  (dotted lines).

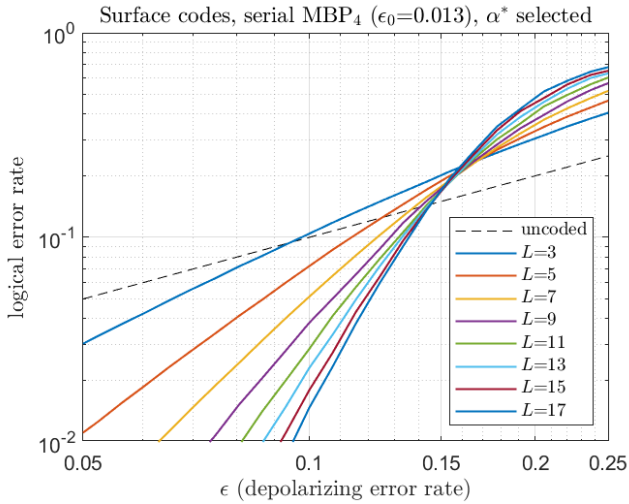


FIG. 16. Serial  $\text{MBP}_4(\alpha^*)$  on surface codes achieves a threshold of 14.5%–16%. The dashed line stands for no error correction (logical error rate  $= \epsilon$ ).

especially when the degeneracy comes from low-weight stabilizers. This demonstrates how the proposed scheme  $\text{MBP}_4$  exploits the degeneracy of surface codes.

Several BDD performance curves at  $L = 17$  are provided in Fig. 13 for reference. Gallager expected BP to have performance around  $1 \times \text{BDD}$  to  $2 \times \text{BDD}$  [30]. Serial  $\text{MBP}_4$  with  $\alpha = 0.65$  has achieved this. However, this is not enough for surface codes. Consider the  $r \times \text{BDD}$  performance curves for  $[[L^2, 1, L]]$  codes at  $r = 1, 2, 3$  in Fig. 14. The depolarizing rate at which the curves corresponding to the same value of  $r$  intersect is called the “BDD error threshold” for the  $[[L^2, 1, L]]$  codes. The theoretical error threshold for a two-dimensional code is 18.9% [48, 58, 59], and thus we would need a decoder with correction radius up to  $0.189N$ , i.e., an  $r \times \text{BDD}$  with  $r$  scaled as  $0.189\sqrt{N} \times 2$ . In other words, as  $L$  increases, an optimum decoder needs to correct most errors in a radius roughly equal to  $0.189N$ , despite that the minimum

distance only scales with  $\sqrt{N}$ . The  $(0.189\sqrt{N} \times 2) \times \text{BDD}$  curves are also drew in Fig. 14 (bold lines) and their intersection seems to suggest an error threshold of 18.9%.

We observed that the performance of  $\text{MBP}_4$  on surface codes saturates for large  $L$ , i.e., the slope of the performance curve does not increase when  $L$  gets larger. There is a similar phenomenon for the neural BP [38, Fig. 4(b)]. Using Algorithm 2 with  $\{\alpha_i\}_{i=1}^L = \{1.0, 0.99, \dots, 0.5\}$ , we have much improved performance for  $L = 17$  by  $\text{MBP}_4(\alpha^*)$  as shown in Fig. 13 at the cost of higher computation complexity.

Note that a maximum number of 150 iterations is allowed in the simulations so that serial  $\text{MBP}_4$  with a fixed  $\alpha$  can perform better. If a proper  $\alpha^*$  can be selected, the maximum number of iterations can be reduced quite a lot (e.g., 30 iterations) without significant performance loss. In fact, sometimes it is possible to use a smaller value of  $\alpha$  instead of the  $\alpha^*$  above, and the convergence can be even faster and remain correct. We will shortly discuss this possibility in Eq. (B1) in Appendix B.

Next we explain how  $\text{MBP}_4$  has the improvement over conventional  $\text{BP}_4$ . Consider serial  $\text{MBP}_4$  with  $\alpha = 0.65$ . We examine the types of corrected errors as in Eq. (21). We plot the ratio of  $n_e/n_0$  in Fig. 15(a). This ratio becomes smaller if the decoder can exploit the degeneracy, which is indeed the case of  $\text{MBP}_4$  in Fig. 15(a). For (conventional)  $\text{BP}_4$ , it has  $n_e/n_0 \approx 1$ ; on the other hand, it also has undetected error rate  $\approx 0$  for large enough  $L > 7$ . Thus the improvement of serial  $\text{MBP}_4$  over  $\text{BP}_4$  comes at a cost of non-negligible undetected error rate, as shown in Fig. 15(b). (A similar phenomenon was also observed in the neural BP decoder [38, Fig. 2(d)].) This unwanted phenomenon is expected, since we use a large step-size so BP may jump far to a logical error (a black solid circle in Fig. 2(b)). However, this is not a random search, or otherwise the ratio  $n_e/n_0$  would be as large as  $1 - (1/2^{2K}) = 3/4$ . Also observe that, in Fig. 15(b), the undetected error rate becomes smaller as  $L$  increases.

The average numbers of iterations are shown in Fig. 15(c). Serial  $\text{MBP}_4$  spends lower average numbers



of iterations (which means a much lower complexity), while conventional  $\text{BP}_4$  spends much more. It means that the improvement comes from a better convergence behavior rather than spending more complexity on, e.g., doing more iterations.

The performance of serial  $\text{MBP}_4$  on toric codes is similar and will be given in Appendix B 3.

Figure 16 is provided for observing the decoding threshold. If a proper value of  $\alpha^*$  can be selected, a threshold of  $14.5\% \leq \epsilon_{\text{surf}} \leq 16\%$  is observed for surface codes. (A threshold of  $14.5\% \leq \epsilon_{\text{toric}} \leq 17.5\%$  is observed for toric codes in Appendix B 3.)

## V. CONCLUSION AND FUTURE RESEARCH

We analyzed the energy topology of BP and proposed a BP algorithm for decoding quantum codes that efficiently explores the degeneracy and significantly improve the performance, especially for highly-degenerate codes. The algorithm has a good convergence performance and a nearly linear complexity in the code length. To further improve  $\text{MBP}_4$ , one may try to analyze the behavior of those uncorrected errors.

Considering BP as an RNN, our proposed scheme has adjustable neuron gains (gradient decent step-size) controlled by  $\alpha$  and fixed inhibition strength. The network introduces a proper memory effect, allowing BP to resist the wrong belief or accelerate the search.

One may introduce additional parameters  $\alpha_{mn,i}$  and  $\beta_{mn,i}$  for each edge  $(m,n)$  and even each iteration  $i$ , but this would require us to develop a strategy of choosing these parameters. In Algorithm 1, there are more useful edges (e.g., the dotted lines in Fig. 4 (a)) not considered in BP-based neural networks [38, 49]. With these added edges, an MBP-based neural network may be considered. The energy function can be defined as in Eq. (7) or any appropriate one. For training the edge weights  $\alpha_{mn,i}$  and  $\beta_{mn,i}$ , their initial values are important [51]. Our simulation results suggest that  $(\alpha_{mn,i}, \beta_{mn,i})$  can be initialized as  $(\alpha, 0)$ , with possible disturbance if needed.

If a proper value of  $\alpha^*$  can be selected,  $\text{MBP}_4$  can achieve decoding thresholds of 14.5%–16% and 14.5%–17.5% for surface and toric codes, respectively.

An efficient strategy to select  $\alpha^*$  would be desired. To determine  $\alpha^*$ , the information of the target error syndrome could be useful. For example, a syndrome vector of high weight would usually correspond to an error of high weight and a smaller value of  $\alpha$  should be chosen.

We note that estimating  $\alpha$  may be estimated by density evolution (DE) [67, 68, 72, 73] or extrinsic information transfer (EXIT) charts [74–76]. (See also some other methods mentioned in [74]). However, cycles in the Tanner graph may affect the accuracy of these methods [68, 76]. With cycles, [68] suggested to consider a method in [77], which estimated the step-size for the first iteration and emphasized its importance. What we did in Sec. III B (and Fig. 3) also serves for this purpose.

We remark that surface (or toric) codes can be decoded by  $\text{MBP}_4$  with a good parallelism. For example, consider the  $[[16, 2, 4]]$  toric code in Fig. 12 (b). The qubits can be divided into four groups  $\{1, 2, 5, 6\}$ ,  $\{3, 4, 7, 8\}$ ,  $\{9, 10, 13, 14\}$ , and  $\{11, 12, 15, 16\}$ . Then the qubits in each group can be decoded in a serial order, while all groups can be run simultaneously. Keeping a group size of four, we will have  $N/4$  groups, which if run with parallelism would have  $O(N/(N/4)) = O(1)$  decoding time. We apply this decoding order for surface codes and a threshold of  $14.5\% \leq \epsilon_{\text{surf}} \leq 15.5\%$  is achieved.

Our scalar-based approach could be extended to the case of fault tolerant circuits. We have an initial study in the data and syndrome error model [52]. Extending this to the fully fault-tolerant model is our ongoing work.

## Appendix A: Linear-domain MBP

Algorithm 3 provides the  $\text{MBP}_4$  in linear domain. The practical complexity can be improved as in Remark 2.

## Appendix B: More simulation results

### 1. Bicycle codes

Herein we provide more simulations for  $[[3786, 946]]$  quantum bicycle codes with various row-weight 24, 20, 16, or 12 in Figs. 17 (a)–(d), respectively. The maximum number of iterations is 90. These results match our expectation that a smaller physical error rate  $\epsilon$  needs a larger  $\alpha$  for better decoding performance (cf. Fig. 3).

### 2. Surface codes

We provide two examples of the decoding on  $L = 7$  surface code in Fig. 18 (a)–(c) and (d)–(f).

The first case is an error of weight 7 as in Fig. 18 (a). The error  $X$  on qubit 4 anticommutes with stabilizer  $Z_3 Z_4 Z_{10} Z_{11}$ , so the corresponding syndrome bit is 1. Conventional  $\text{BP}_4$  (parallel  $\text{BP}_4$ ) cannot decide whether an error  $X$  is on qubit 3 or qubit 4. To break this symmetry, possible methods include post-processes (random perturbation [32], OSD [33, 34], etc) or pre-processes (like training [36–39]). On the other hand, using serial  $\text{MBP}_4$  with  $\alpha = 0.65$  can make correct decision without additional processes. (It will decide an error  $X$  at qubit 3.)

Now we consider the complete error set on the surface code in Fig. 18 (a). The update of the estimated error at each iteration is shown in Table III for various combinations of BP decoding. It shows that parallel  $\text{MBP}_4$  with  $\alpha = 0.65$  oscillates between two states. In this case, using a serial schedule (serial  $\text{MBP}_4$  with  $\alpha = 0.65$ ) can soon make it converge.

Parallel  $\text{BP}_4$  traps around an error of smaller weight, as shown in Fig. 18 (b) and Table III. The reason that it

---

**Algorithm 3 :** MBP<sub>4</sub> in linear domain (with  $\beta = 0$ )

---

**Input:**  $S \in \{I, X, Y, Z\}^{M \times N}$ ,  $z \in \{0, 1\}^M$ ,  $T_{\max} \in \mathbb{Z}_+$ , a real  $\alpha > 0$ , and initial beliefs  $\{p_n = (p_n^I, p_n^X, p_n^Y, p_n^Z) \in \mathbb{R}^4\}_{n=1}^N$ .

**Initialization.** For  $n = 1, 2, \dots, N$  and  $m \in \mathcal{M}(n)$ , let

$$d_{n \rightarrow m} = q_{n \rightarrow m}^{(0)} - q_{n \rightarrow m}^{(1)},$$

where  $q_{n \rightarrow m}^{(0)} = p_n^I + p_n^{S_{mn}}$  and  $q_{n \rightarrow m}^{(1)} = 1 - q_{n \rightarrow m}^{(0)}$ .

**Horizontal Step.** For  $m = 1, 2, \dots, M$  and  $n \in \mathcal{N}(m)$ , compute

$$\delta_{m \rightarrow n} = (-1)^{z_m} \prod_{n' \in \mathcal{N}(m) \setminus n} d_{n' \rightarrow m},$$

**Vertical Step.** For  $n = 1, 2, \dots, N$  and  $m \in \mathcal{M}(n)$ , do:

- Compute

$$r_{m \rightarrow n}^{(0)} = \left(\frac{1 + \delta_{m \rightarrow n}}{2}\right)^{1/\alpha}, \quad r_{m \rightarrow n}^{(1)} = \left(\frac{1 - \delta_{m \rightarrow n}}{2}\right)^{1/\alpha}, \quad (23)$$

$$q_{n \rightarrow m}^W = p_n^W \prod_{m' \in \mathcal{M}(n) \setminus m} r_{m' \rightarrow n}^{(\langle W, S_{m'n} \rangle)}, \quad W \in \{I, X, Y, Z\}.$$

- Let

$$\begin{aligned} q_{n \rightarrow m}^{(0)} &= a_{mn} (q_{n \rightarrow m}^I + q_{n \rightarrow m}^{S_{mn}}) / \left(\frac{1 + \delta_{m \rightarrow n}}{2}\right)^{1-1/\alpha}, \\ q_{n \rightarrow m}^{(1)} &= a_{mn} (\sum_{W'} q_{n \rightarrow m}^{W'}) / \left(\frac{1 - \delta_{m \rightarrow n}}{2}\right)^{1-1/\alpha}, \end{aligned} \quad (24)$$

where  $W' \in \{X, Y, Z\} \setminus S_{mn}$  and  $a_{mn}$  is a chosen scalar such that  $q_{n \rightarrow m}^{(0)} + q_{n \rightarrow m}^{(1)} = 1$ .

- Update:  $d_{n \rightarrow m} = q_{n \rightarrow m}^{(0)} - q_{n \rightarrow m}^{(1)}$ .

**Hard Decision.** For  $n = 1, 2, \dots, N$ , compute

$$q_n^W = p_n^W \prod_{m \in \mathcal{M}(n)} r_{m \rightarrow n}^{(\langle W, S_{mn} \rangle)}, \quad W \in \{I, X, Y, Z\}.$$

Let  $\hat{E} = \hat{E}_1 \hat{E}_2 \dots \hat{E}_N$ , where  $\hat{E}_n = \arg \max_{W \in \{I, X, Y, Z\}} q_n^W$ .

- If  $\langle \hat{E}, S_m \rangle = z_m \forall m$ , halt and return “CONVERGE”;
  - otherwise, if the maximum number of iterations  $T_{\max}$  is reached, halt and return “FAIL”;
  - otherwise, repeat from the horizontal step.
- 

is easy to trap near the origin is explained in Fig. 2. On the other hand, serial MBP<sub>4</sub> with  $\alpha < 1$  performs a fast asymmetric update with large step-size. It performs a very aggressive search without jumping wrongly (as shown in Table III), and finally converges to a valid degenerate error, as shown in Fig. 18(c). The error in Fig. 18(c) is equivalent to the error in Fig. 18(a) up to three stabilizers  $X_3 X_4$ ,  $Z_{15} Z_{16} Z_{22} Z_{23}$ , and  $X_{32} X_{33} X_{39} X_{40}$ .

In the second case, two more  $X$  errors on qubits 6 and 7 are added. Now the overall error is of weight  $9 > D = 7$  as in Fig. 18(d). There is a similar result that conventional BP<sub>4</sub> traps around a smaller weight as shown in Fig. 18(e). Serial MBP<sub>4</sub> with  $\alpha < 1$  finds a

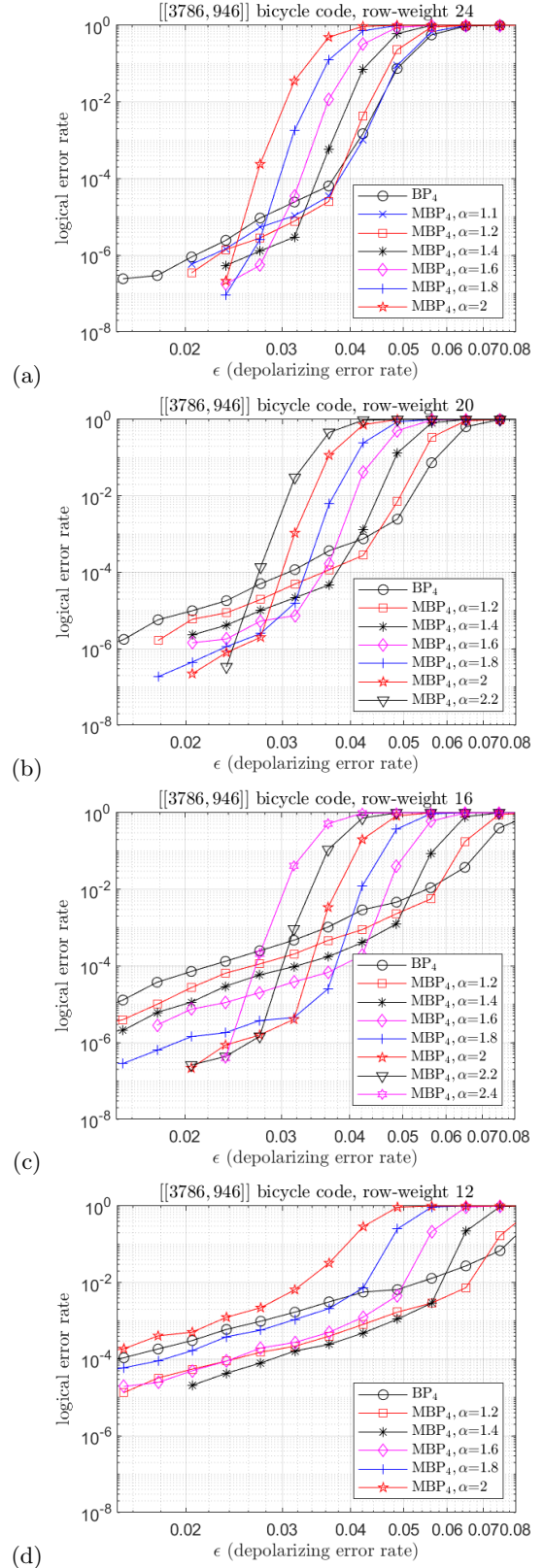


FIG. 17. Performance of parallel BP<sub>4</sub> and MBP<sub>4</sub> on the [[3786, 946]] bicycle codes with different row-weights  $k$ , based on  $T_{\max} = 90$ . (a)  $k = 24$ . (b)  $k = 20$ . (c)  $k = 16$ . (d)  $k = 12$ . The trend of the curves can be explained as in Sec. III B (and Fig. 3).

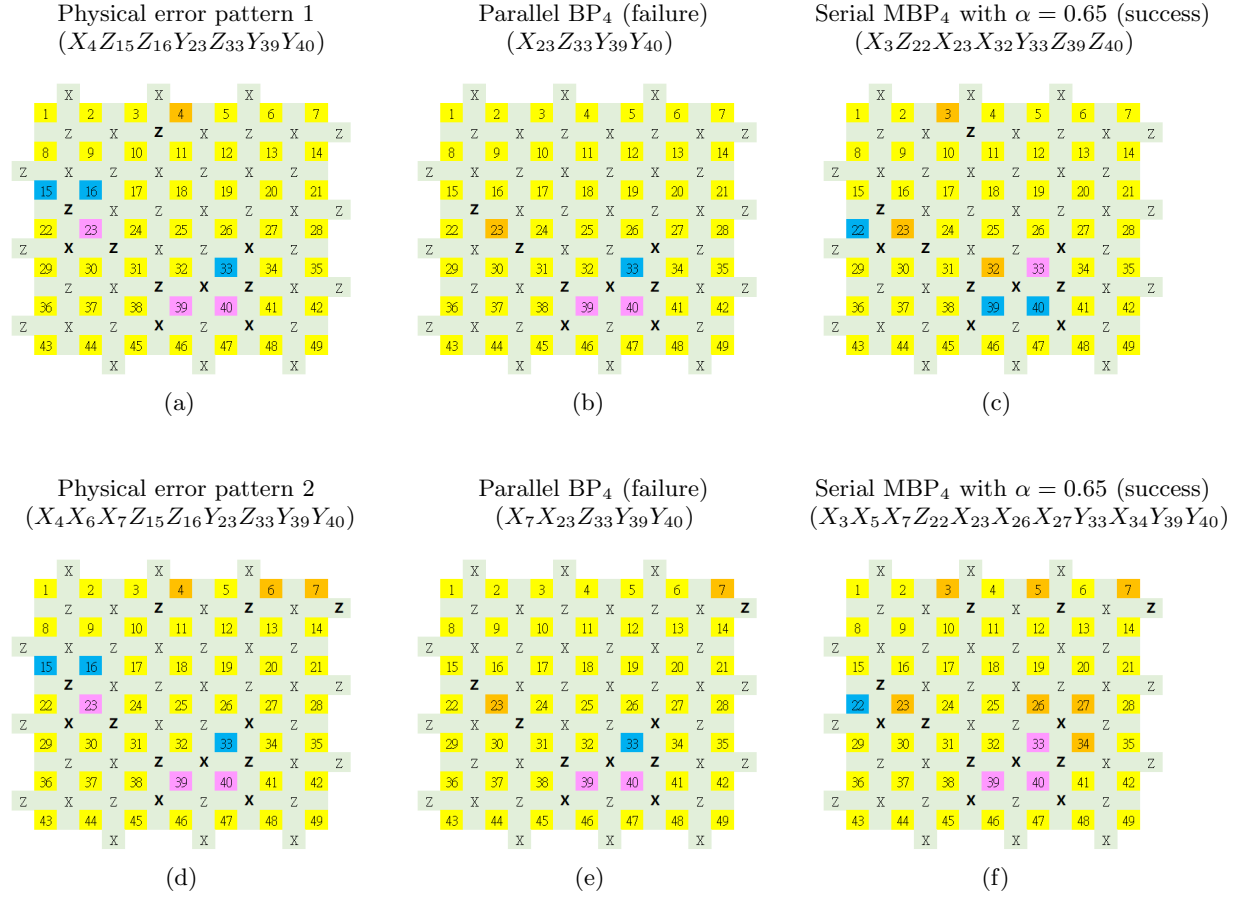


FIG. 18. Two examples of the  $L = 7$  surface code: (a)–(c) the first case and (d)–(f) the second case. A clean qubit is denoted by a numbered yellow box. If a qubit suffers an  $X$ ,  $Y$ , or  $Z$  error, it is denoted by an orange, purple, or blue box, respectively. A stabilizer is denoted by an  $X$  or  $Z$ . If the corresponding syndrome bit is 1, it is bold-faced. Figures (a) and (d) are the actual error patterns, (b) and (e) are the decoding results of conventional  $BP_4$  (which are failures with unmatched syndromes), and (c) and (f) are the decoding results of serial  $MBP_4$  with  $\alpha = 0.65$  (which are degenerate errors of those in (a) and (d)).

TABLE III. The estimated error  $\hat{E}$  of the first example Fig. 18(a) at each iteration (iter.) in Figs. 18(b) and 18(c), and various configurations in between.

iter.	(b) Parallel $BP_4$	Parallel normalized $BP_4$ with $\alpha_c = 0.65$	Parallel $MBP_4$ with $\alpha = 0.65$
1	$Y_{23}X_{31}Y_{33}Y_{39}Y_{40}$	$X_3X_4Z_{22}Y_{23}Z_{29}X_{31}Y_{33}Y_{39}Y_{40}$	$X_3X_4Z_{22}Y_{23}Z_{29}X_{31}Y_{33}Y_{39}Y_{40}$
2	$X_{23}Y_{33}Y_{39}Y_{40}$	$X_3X_4X_{10}Z_{22}X_{23}Z_{24}Y_{29}Z_{30}Y_{31}X_{32}Y_{33}Y_{39}Y_{40}$	$X_{23}Y_{29}Y_{33}Y_{39}Y_{40}$
3	$X_{23}Z_{33}Y_{39}Y_{40}$	$X_3X_4X_{16}Y_{22}Y_{24}X_{25}Z_{29}Y_{30}Z_{33}Y_{39}Y_{40}$	$X_3X_4Y_{22}X_{23}Z_{29}Z_{33}Y_{39}Z_{40}$
4	$Y_{22}X_{23}Z_{33}Y_{39}Y_{40}$	$X_3X_4Y_{18}Z_{10}Z_{15}X_{16}Z_{18}Z_{25}Z_{31}Z_{32}Z_{33}Z_{39}Y_{40}$	$X_{10}X_{23}Z_{33}Z_{39}Y_{40}$
5	$X_{23}Z_{33}Y_{39}Y_{40}$	$Y_9X_{10}X_{16}Z_{26}Z_{30}X_{31}Y_{33}Z_{38}Y_{39}Y_{40}$	$Z_{22}X_{23}Z_{29}Z_{33}Y_{39}Y_{40}$
6	$X_{23}Z_{33}Y_{39}Y_{40}$	$X_4X_{10}Y_{16}Z_{18}X_{27}Z_{33}Y_{39}Z_{40}Y_{44}X_{48}X_{49}$	$X_3X_4X_{23}Z_{33}Y_{39}Y_{40}$
7	$X_{23}Z_{33}Y_{39}Y_{40}$	$X_3X_4X_{10}Y_{17}Z_{22}Y_{23}Y_{24}Z_{29}Y_{31}Z_{39}Y_{40}$	$Z_{22}X_{23}Z_{29}Z_{33}Y_{39}Y_{40}$
8	$X_{23}Z_{33}Y_{39}Y_{40}$	$X_{17}Y_{23}Z_{29}Y_{31}Y_{33}Z_{34}Z_{39}Y_{40}$	$X_3X_4X_{23}Z_{33}Y_{39}Y_{40}$
9	$X_{23}Z_{33}Y_{39}Y_{40}$	$X_3X_4X_{10}Z_{16}Z_{21}X_{22}Z_{23}Y_{24}Y_{26}Z_{27}Z_{28}Y_{30}X_{32}Z_{33}Y_{38}Y_{39}Z_{40}Z_{41}Y_{46}X_{47}$	$Z_{22}X_{23}Z_{29}Z_{33}Y_{39}Y_{40}$
10	$X_{23}Z_{33}Y_{39}Y_{40}$	$Z_{17}Z_{41}X_{10}Y_{16}Y_{25}Y_{26}X_{27}Z_{30}Z_{31}Y_{32}X_{33}X_{34}X_{37}X_{40}X_{42}Y_{44}Y_{46}Y_{47}$	$X_3X_4X_{23}Z_{33}Y_{39}Y_{40}$
11	... (Trap here)	... (Diverge)	... (Oscillate)
iter.	Serial $BP_4$	Serial normalized $BP_4$ with $\alpha_c = 0.65$	(c) Serial $MBP_4$ with $\alpha = 0.65$
1	$X_{23}Y_{33}$	$X_3X_4X_5X_6X_7Z_{22}Y_{23}Z_{29}X_{31}Y_{33}Y_{39}Y_{40}$	$X_3Z_{22}X_{23}Y_{33}Y_{40}$
2	$X_{23}X_{31}X_{32}Y_{33}Z_{38}Y_{39}$	$X_3X_4X_5X_6X_7X_{10}X_{11}X_{12}X_{13}X_{14}Z_{22}X_{23}Z_{24}Y_{29}Z_{30}Y_{31}X_{32}Y_{33}Y_{39}Y_{40}$	$X_3X_{23}Z_{29}Z_{30}X_{32}Y_{33}Z_{38}Z_{39}Z_{40}$
3	$Y_{29}Y_{30}Z_{33}Y_{39}Y_{40}$	$X_3X_4X_7X_{11}X_{12}X_{13}X_{14}X_{16}Y_{22}Y_{24}X_{25}Z_{29}Y_{30}Z_{33}Y_{39}Z_{40}$	$X_{23}Z_{30}Y_{33}Y_{39}Y_{40}$
4	$Y_{22}Z_{33}Y_{39}Y_{40}$	$Y_8Z_{10}Y_{11}X_{13}X_{14}Z_{15}X_{16}Z_{18}Z_{25}Z_{31}Z_{32}Z_{33}Z_{39}Y_{40}$	$X_3X_{23}X_{32}Z_{33}Z_{39}Z_{40}$
5	$X_{23}Z_{33}Y_{39}Y_{40}$	$Y_9Y_{12}X_{16}X_{23}Z_{26}Z_{30}X_{31}Y_{33}Z_{38}Y_{39}Y_{40}$	$X_3Z_{22}X_{23}Z_{33}X_{34}Y_{39}Y_{40}$
6	$X_{23}Z_{33}Y_{39}Y_{40}$	$X_4X_7Y_{13}Y_{16}Z_{18}Z_{19}Y_{20}X_{27}Y_{28}Z_{30}Z_{33}Y_{39}Z_{40}Y_{44}X_{48}X_{49}$	$X_3Z_{22}X_{23}X_{25}X_{26}X_{27}X_{32}Y_{33}X_{34}Z_{39}Z_{40}X_{46}$
7	$X_{23}Z_{33}Y_{39}Y_{40}$	$X_3X_4Y_7X_{10}Y_{13}Y_{17}X_{21}Y_{23}Y_{24}Y_{31}Z_{39}Y_{40}$	$X_3X_{17}Z_{22}X_{23}X_{24}X_{26}X_{27}X_{31}Z_{33}Z_{39}Z_{40}$
8	$X_{23}Z_{33}Y_{39}Y_{40}$	$X_7Y_{10}X_{17}Y_{23}Z_{27}Y_{31}Z_{32}Z_{33}Z_{34}Y_{39}Y_{40}$	$X_3X_{10}Z_{22}X_{23}X_{26}X_{32}Y_{33}Z_{39}Z_{40}$
9	$X_{23}Z_{33}Y_{39}Y_{40}$	$X_3X_4X_5X_6X_7X_{10}X_{14}Z_{21}X_{23}Z_{24}Y_{26}Z_{28}Y_{33}Y_{34}Z_{38}Y_{39}Y_{40}Z_{41}Y_{46}X_{47}$	$X_{11}Z_{22}X_{23}X_{32}Y_{33}Z_{39}Z_{40}$
10	$X_{23}Z_{33}Y_{39}Y_{40}$	$Z_{17}Z_{41}X_{10}Y_{16}Y_{25}Y_{26}X_{27}Y_{28}Z_{30}Z_{31}Y_{32}X_{33}X_{34}X_{37}X_{40}X_{42}Y_{44}Y_{46}X_{48}X_{49}$	$X_3Z_{22}X_{23}X_{32}Y_{33}Z_{39}Z_{40}$
11	... (Trap here)	... (Diverge)	(Converged, a valid degenerate error)

valid degenerate error (of larger weight 11) as shown in Fig. 18(f), which is equivalent to the error in Fig. 18(d) up to four stabilizers  $X_3X_4$ ,  $X_5X_6$ ,  $Z_{15}Z_{16}Z_{22}Z_{23}$ , and  $X_{26}X_{27}X_{33}X_{34}$ .

For demonstration of the effects of smaller  $\alpha$ , we run

serial  $MBP_4$  with  $\alpha = 0.5$  on the two examples. In each

case, the decoding correctly converges in two iterations:

$$\begin{aligned} \text{MBP}_4(\alpha = 0.5) \text{ on case (a): } & \rightarrow X_3 Z_{22} X_{23} Y_{33} X_{39} Y_{40} \\ & \rightarrow X_3 X_{23} Z_{29} X_{32} Y_{33} Z_{39} Z_{40}. \\ \text{MBP}_4(\alpha = 0.5) \text{ on case (d): } & \rightarrow X_3 X_5 X_7 Z_{22} X_{23} Y_{33} X_{39} Y_{40} \\ & \rightarrow X_3 X_5 X_7 X_{23} Z_{29} X_{32} Y_{33} Z_{39} Z_{40}. \end{aligned} \quad (\text{B1})$$

The first result in Eq. (B1) is equivalent to the error in Fig. 18(a) up to four stabilizers  $X_3 X_4$ ,  $Z_{15} Z_{16} Z_{22} Z_{23}$ ,  $Z_{22} Z_{29}$ , and  $X_{32} X_{33} X_{39} X_{40}$ . The second result in Eq. (B1) is equivalent to the error in Fig. 18(d) up to five stabilizers  $X_3 X_4$ ,  $X_5 X_6$ ,  $Z_{15} Z_{16} Z_{22} Z_{23}$ ,  $Z_{22} Z_{29}$ , and  $X_{32} X_{33} X_{39} X_{40}$ . This suggests that using a smaller  $\alpha$  may have a faster and yet correct convergence.

Note that, as shown in Table III, using normalized BP<sub>4</sub> with  $\alpha_c < 1$  makes the decoding diverge. This can also be observed by monitoring the variation of the energy function and we will discuss it in Appendix C.

### 3. Toric codes

Now we give the decoding performance for  $[[L^2, 2, L]]$  toric codes with even  $L$ . An example of the toric code lattice is shown in Fig. 12(b). Note that a toric code has every stabilizer generator associated with four qubits, and every qubit involved in four stabilizer measurements, so the corresponding check matrix is completely symmetric. This makes the toric code more suitable to have the same  $\alpha$  for all the edges.

Figure 20 provides the simulation results of the toric codes with various distances. Due to the symmetry of the check matrix, the performance of each toric code is generally better than the surface code of comparable size in Fig. 13. Note that the performance curve of BP has no fluctuation with or without fixed initialization.

Our simulations suggest to use  $\alpha = 0.75$  in MBP<sub>4</sub> for better performance, which is larger than  $\alpha = 0.65$  used for surface codes (Fig. 13). Since a toric code has a fixed row-weight 4, which is larger than the mean row-weight (between 2 and 4) of a surface code, this agrees to the observation in Fig. 3 that a code with a larger row-weight should choose a larger  $\alpha$ .

Similar to Fig. 13, there is the phenomenon of performance saturation when  $L$  gets larger. This can be improved by MBP<sub>4</sub>( $\alpha^*$ ) using Algorithm 2 with  $\{\alpha_i\}_{i=1}^L = \{1.0, 0.99, \dots, 0.5\}$ . We show this by  $L = 18$  with  $\alpha^*$  selected during decoding, and the decoder corrects most errors within  $4 \times \text{BDD}$  correction radius. This is better than a comparable case “ $L = 17$  with  $\alpha^*$  selected” in Fig. 13, where roughly  $3 \times \text{BDD}$  performance is achieved.

By initializing  $\Lambda$  with respect to a fixed  $\epsilon_0 = 0.001$  in MBP<sub>4</sub>, we get a slightly better interpolation performance for large  $\epsilon$  so we apply this technique in MBP<sub>4</sub>( $\alpha^*$ ).

Similar to Fig. 15, we provide some statistics for decoding toric codes in Fig. 19. Again, serial MBP<sub>4</sub> with  $\alpha < 1$  significantly improves conventional BP<sub>4</sub> by exploiting the degeneracy as shown (Fig. 19(a)) at the cost

of having some undetected errors (Fig. 19(b)), and it has better algorithm convergence (Fig. 19(c)).

By using serial MBP<sub>4</sub>( $\alpha^*$ ) on toric codes, we observe a threshold of 14.5%–17.5% as shown in Fig. 21.

### Appendix C: Energy function

We may consider a bounded  $\tilde{J}_S$  from  $J_S$  in Eq. (8) by

$$\tilde{J}_S = - \sum_{m=1}^M \tilde{\Delta}_m \approx - \sum_{m=1}^M \Delta_m, \quad (\text{C1})$$

where  $\Delta_m = 2 \tanh^{-1} \left( (-1)^{z_m} \prod_{n \in \mathcal{N}(m)} \tanh \left( \frac{\lambda_{S_{mn}}(\Gamma_n)}{2} \right) \right)$

and  $\tilde{\Delta}_m \approx \Delta_m$  but bounded as

$$\tilde{\Delta}_m = \text{sign}(\Delta_m) \min\{|\Delta_m|, B\} \quad (\text{C2})$$

for some positive  $B$ .

Note that if we define, in linear domain,

$$\delta_m = \prod_{n \in \mathcal{N}(m)} \left( (q_n^I + q_n^{S_{mn}}) - (\sum_{W \in \{X, Y, Z\} \setminus S_{mn}} q_n^W) \right)$$

from the output distribution in Algorithm 3, then  $\Delta_m = \ln \frac{1+\delta_m}{1-\delta_m}$  and  $B = 6$  can cover  $|\delta_m| \leq 0.99$  since  $\ln \frac{1+0.99}{1-0.99} \approx 5.3 < 6$ .

To have a differentiable function, we consider a Taylor expansion of  $\Delta_m = \ln \frac{1+\delta_m}{1-\delta_m}$  at  $\delta_m = 0$  as

$$\tilde{\Delta}_m^{(l)} = 2 \left( \delta_m + \frac{\delta_m^3}{3} + \frac{\delta_m^5}{5} + \dots + \frac{\delta_m^l}{l} \right) \quad (\text{C3})$$

with a finite order  $l \geq 1$ . Let the corresponding approximation of  $J_S$  be  $\tilde{J}_l$ , defined by

$$\tilde{J}_l = - \sum_{m=1}^M \tilde{\Delta}_m^{(l)} = -2 \sum_{m=1}^M \left( \delta_m + \frac{\delta_m^3}{3} + \frac{\delta_m^5}{5} + \dots + \frac{\delta_m^l}{l} \right). \quad (\text{C4})$$

Even by using  $l = 1$ , the function

$$\tilde{J}_1 = -2 \sum_{m=1}^M \delta_m, \quad (\text{C5})$$

up to a scalar of 2, is sufficient to be an energy function for the classical syndrome based-decoding (cf. Lemma 2 and (21) in [40]). However,  $l$  needs to be large for a good approximation of  $J_S$ .

Since a target  $\delta_m > 0$  (a target  $\Delta_m > 0$ ), we may also consider another energy function to focus on negative  $\Delta_m$  (i.e., to focus on mismatched checks) by

$$\bar{J}_S = \sum_{m=1}^M \min\{0, \Delta_m\}. \quad (\text{C6})$$

This energy function  $\bar{J}_S$  can be simplified as  $\dot{J}_S$  that counts the number of unmatched checks

$$\dot{J}_S = \sum_{m=1}^M \min\{0, \text{sign}(\Delta_m)\} = - \sum_{m=1}^M |z_m - \hat{z}_m|, \quad (\text{C7})$$

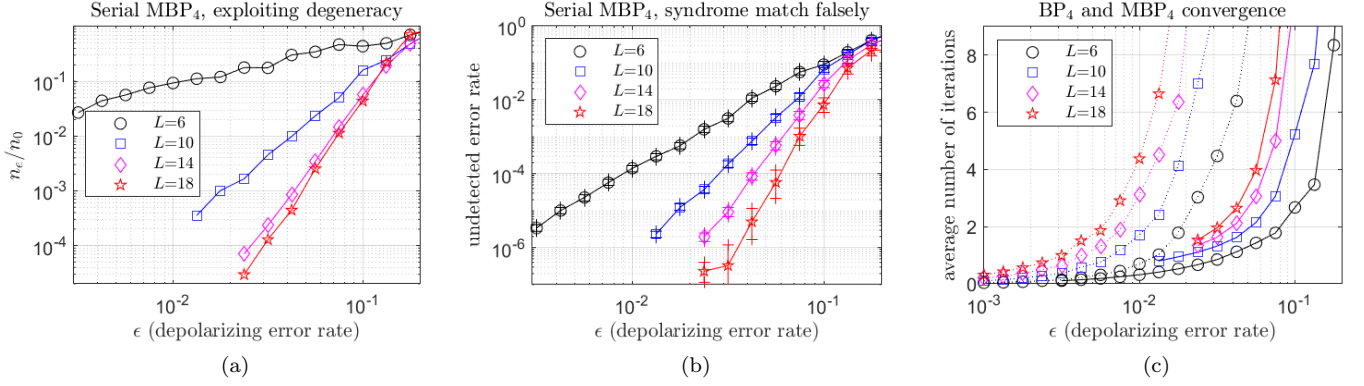


FIG. 19. Some statistics of decoding toric codes using serial MBP<sub>4</sub> with  $\alpha = 0.75$  (solid lines). (a) The ratio  $n_e/n_0$ . (b) Undetected error rate. (c) Average numbers of iterations; also shown in (c) are the numbers for conventional BP<sub>4</sub> (dotted lines).

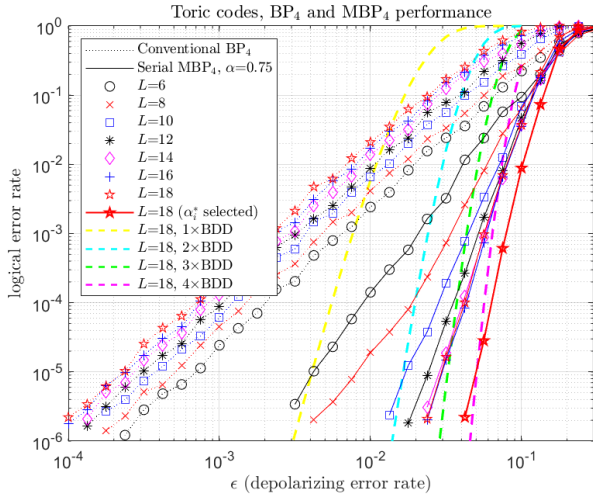


FIG. 20. Conventional BP<sub>4</sub> and serial MBP<sub>4</sub> decoding performance on toric codes, based on  $T_{\max} = 150$ . The curve corresponding to  $\alpha^*$  is generated by fixed initialization with  $\epsilon_0 = 0.001$ , instead of the  $\epsilon$  that generates the depolarizing errors (as discussed in Remark 4).

where  $\hat{z}_m = \langle \hat{E}, S_m \rangle$ . This energy function is used by a simplified BP called bit-flipping BP [30, 31, 35, 78, 79], which decides the update direction (which bit to flip) by minimizing the number of unmatched syndrome bits between  $z$  and  $\hat{z}$ . Bit-flipping BP has very low complexity and is useful for analyzing the convergence, since it only tracks the hard-decision information of the variable nodes. (Bit-flipping BP can also be used in practice, e.g., it was used in decoding expander codes [78].)

To see the difference of the energy functions discussed above, we provide an example in Fig. 22.

For decoding the error pattern in Fig. 18(a), we plot the change of the energy function for the six configurations in Table III. First, we consider the approximated  $\tilde{J}_S$  in (C1) with  $B = 6$ , with the result plotted

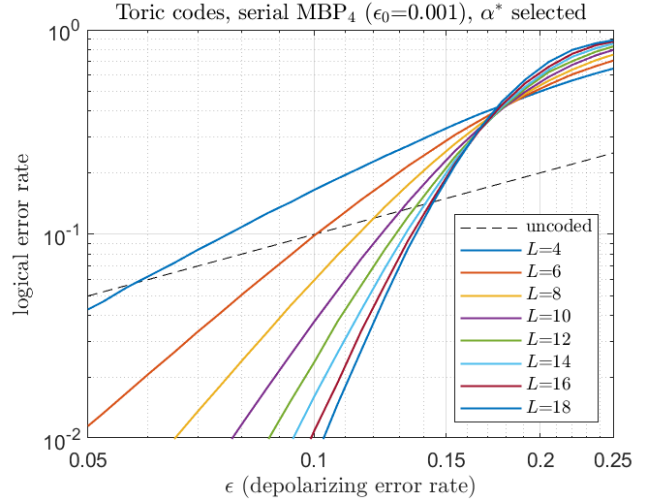


FIG. 21. Serial MBP<sub>4</sub>( $\alpha^*$ ) on toric codes achieves a threshold of 14.5%–17.5%. The dashed line stands for no error correction (logical error rate =  $\epsilon$ ).

in Fig. 22(a). Conventional BP<sub>4</sub> (no matter parallel or serial) has achieved low energy, though the decoding is not successful. If changed to a larger step-size by using normalized BP<sub>4</sub> with  $\alpha_c = 0.65$ , the decoding then jumps randomly and diverges, resulting in high energy. When using MBP<sub>4</sub> with  $\alpha = 0.65$ , the decoding converges to lowest energy. In this example, serial MBP<sub>4</sub> successfully converges to a degenerate error at iteration 10.

Then we consider the energy function  $\tilde{J}_S$  in (C7), with the result plotted in Fig. 22(b). Only serial MBP<sub>4</sub> finally converges without trapping in local minima. Note that, in Table III, parallel BP<sub>4</sub> has a hard-decision pattern not changed after iteration 5. But the energy  $\tilde{J}_S$  or  $\tilde{J}_S$  can still change. For example, consider the output distribution  $(q_n^I, q_n^X, q_n^Y, q_n^Z)$  to oscillate between two points (0.4, 0.3, 0.25, 0.05) and (0.4, 0.05, 0.25, 0.3); then the hard-decision is the same  $\hat{E}_n = I$  but, e.g., for an

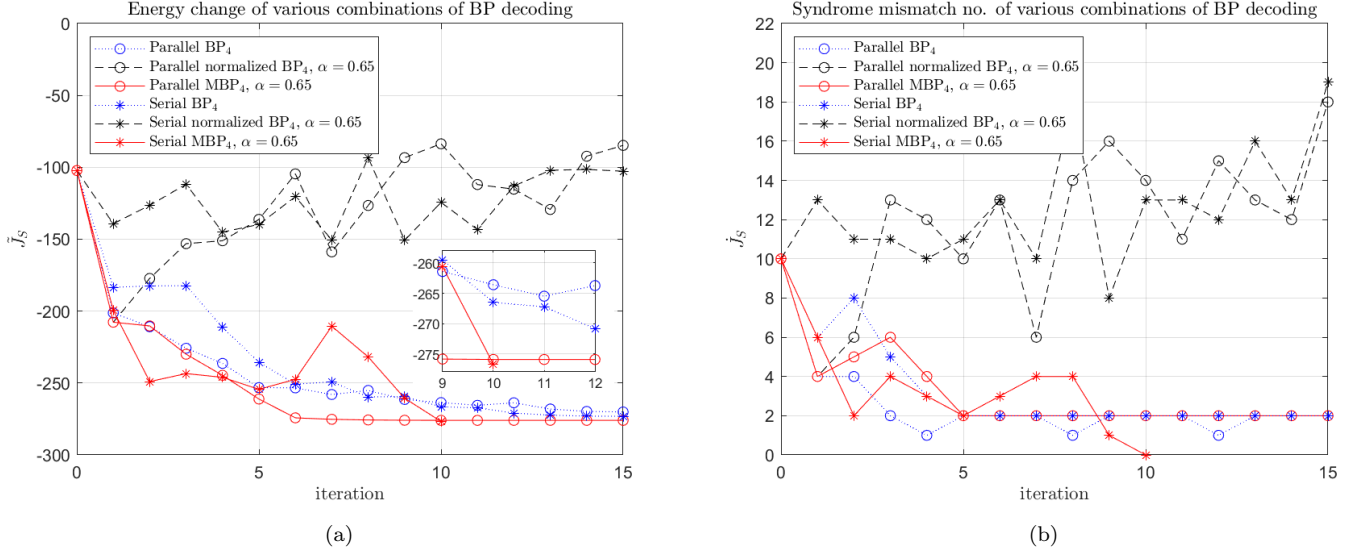


FIG. 22. Plotting the change of the energy function during iterations, for decoding the error pattern in Fig. 18 (a) with the six configurations in Table III. (a) Using  $\tilde{J}_S$  in (C1) with  $B = 6$ . (b) Using  $\tilde{J}_S$  in (C7). Using (C5) or (C6) results in a figure similar to (a). Serial MBP $_4$  with  $\alpha = 0.65$  is the only configuration that achieves a successful decoding (at iteration 10).

edge type  $X$ , the probability  $q_n^I + q_n^X = 0.7 > 0.5$  for the first point and  $q_n^I + q_n^X = 0.45 < 0.5$  for the second point, which can cause different energy levels.

There are two further notes. First, parallel MBP $_4$ , though not finally converged, achieves low energy in both figures. This explains why BP with post-processing usually works.

Second, when we try to plot  $J = J_D + J_S$  (Eq. (7)) rather than  $J_S$  (Eq. (8)), it needs a quite large  $\eta \approx 10^6$  to have a correct trend; or otherwise, a successful decoding may result in high energy level. Having large  $\eta$  matches our expectation since decoding a highly-degenerate code

should more focus on  $J_S$  (where any degenerate errors can lower it) rather than  $J_D$  (where a single low-weight error can dominate it, even if the error does not have correct syndrome).

## ACKNOWLEDGMENTS

CYL was financially supported from the Young Scholar Fellowship Program by the Ministry of Science and Technology (MOST) in Taiwan, under Grant MOST109-2636-E-009-004.

- 
- [1] P. W. Shor, Algorithms for quantum computation: Discrete logarithms and factoring, in *Proc. Annu. Symp. Found. Comput. Sci. (FOCS)* (IEEE, 1994) pp. 124–134.
  - [2] Y. Wang, M. Um, J. Zhang, S. An, M. Lyu, J.-N. Zhang, L.-M. Duan, D. Yum, and K. Kim, Single-qubit quantum memory exceeding ten-minute coherence time, *Nat. Photon.* **11**, 646 (2017).
  - [3] F. Arute, K. Arya, R. Babbush, D. Bacon, J. C. Bardin, R. Barends, R. Biswas, S. Boixo, F. G. Brandao, D. A. Buell, *et al.*, Quantum supremacy using a programmable superconducting processor, *Nature* **574**, 505 (2019).
  - [4] P. W. Shor, Fault-tolerant quantum computation, in *Proc. Annu. Conf. Found. Comput. Sci. (FOCS)* (IEEE, 1996) pp. 56–65.
  - [5] M. Suchara, J. Kubitowicz, A. Faruque, F. T. Chong, C.-Y. Lai, and G. Paz, QuRE: The quantum resource estimator toolbox, in *Proc. IEEE Int. Conf. Comput. Design (ICCD)* (2013) pp. 419–426.
  - [6] D. Gottesman, *Stabilizer codes and quantum error correction*, Ph.D. thesis, Caltech (1997).
  - [7] A. R. Calderbank, E. M. Rains, P. W. Shor, and N. J. A. Sloane, Quantum error correction via codes over GF(4), *IEEE Trans. Inf. Theory* **44**, 1369 (1998).
  - [8] A. Y. Kitaev, Fault-tolerant quantum computation by anyons, *Ann. Phys.* **303**, 2 (2003).
  - [9] C. Horsman, A. G. Fowler, S. Devitt, and R. Van Meter, Surface code quantum computing by lattice surgery, *New J. Phys.* **14**, 123011 (2012).
  - [10] H. Bombin and M. A. Martin-Delgado, Topological quantum distillation, *Phys. Rev. Lett.* **97**, 180501 (2006).
  - [11] D. J. C. MacKay, G. Mitchison, and P. L. McFadden, Sparse-graph codes for quantum error correction, *IEEE Trans. Inf. Theory* **50**, 2315 (2004).
  - [12] J.-P. Tillich and G. Zémor, Quantum LDPC codes with positive rate and minimum distance proportional to the square root of the blocklength, *IEEE Trans. Inf. Theory* **60**, 1193 (2014).
  - [13] A. A. Kovalev and L. P. Pryadko, Quantum Kronecker



- sum-product low-density parity-check codes with finite rate, *Phys. Rev. A* **88**, 012311 (2013).
- [14] K.-Y. Kuo and C.-C. Lu, On the hardnesses of several quantum decoding problems, *Quant. Inf. Process.* **19**, 1 (2020).
  - [15] P. Iyer and D. Poulin, Hardness of decoding quantum stabilizer codes, *IEEE Trans. Inf. Theory* **61**, 5209 (2015).
  - [16] J. Edmonds, Paths, trees, and flowers, *Canadian Journal of Mathematics* **17**, 449 (1965).
  - [17] E. Dennis, A. Kitaev, A. Landahl, and J. Preskill, Topological quantum memory, *J. Math. Phys.* **43**, 4452 (2002).
  - [18] C. Wang, J. Harrington, and J. Preskill, Confinement-Higgs transition in a disordered gauge theory and the accuracy threshold for quantum memory, *Ann. Phys.* **303**, 31 (2003).
  - [19] R. Raussendorf, J. Harrington, and K. Goyal, A fault-tolerant one-way quantum computer, *Ann. Phys.* **321**, 2242 (2006).
  - [20] D. S. Wang, A. G. Fowler, A. M. Stephens, and L. C. L. Hollenberg, Threshold error rates for the toric and planar codes, *Quant. Inf. Comput.* **10**, 456 (2010).
  - [21] A. G. Fowler, A. C. Whiteside, and L. C. Hollenberg, Towards practical classical processing for the surface code, *Phys. Rev. Lett.* **108**, 180501 (2012).
  - [22] A. G. Fowler, Minimum weight perfect matching of fault-tolerant topological quantum error correction in average  $O(1)$  parallel time, *Quant. Inf. Comput.* **15**, 145 (2015).
  - [23] G. Duclos-Cianci and D. Poulin, Fast decoders for topological quantum codes, *Phys. Rev. Lett.* **104**, 050504 (2010).
  - [24] The decoding problem of color codes can be cast as a hypergraph matching problem and approximately solved by MWM with a threshold of 6.25%–13.3% over depolarizing errors [80]. In addition, a color code can be projected to two surface codes and decoded by the combination of RG and BP (RG-BP) [23] with a threshold of 8.7% over bit-flip errors [81]. A color code can be also projected to three surface codes and decoded by MWM with a threshold of 8.7% over bit-flip errors [82]. Alternatively, color codes can be decoded by RG-BP, without the projection on surface codes, with a threshold of 7.8% over bit-flip errors [83]. A summary of the thresholds for various decoders on color codes can be found in [84].
  - [25] K.-Y. Kuo and C.-Y. Lai, Refined belief propagation decoding of sparse-graph quantum codes, *IEEE J. Sel. Area. Inf. Theory* **1**, 487 (2020).
  - [26] K.-Y. Kuo and C.-Y. Lai, Refined belief-propagation decoding of quantum codes with scalar messages, in *Proc. IEEE Globecom Workshops* (2020) pp. 1–6.
  - [27] K.-Y. Kuo and C.-Y. Lai, Log-domain decoding of quantum LDPC codes over binary finite fields, e-print arXiv:2104.00304 (2021).
  - [28] There are several variants of BP (with complexity depending on the variant) such as BP with heuristic post-processing [32] (tested on a bicycle code), RG-BP on toric codes [23], RG-BP on color codes [81, 83], BP-MWM on surface/toric codes [57], BP-OSD on (generalized) bicycle, HP and some topological codes [33, 34], and BP with small set flipping (BP-SSF) on HP codes with expander graphs [85] (where SSF [86, 87] is a generalization of *bit-flipping BP* for classical expander codes [78]).
  - [29] M. Davey and D. MacKay, Low-density parity check codes over  $GF(q)$ , *IEEE Commun. Lett.* **2**, 165 (1998), (see also the conference version, with the same title, in *Proc. IEEE Inf. Theory Workshop (ITW)*, 1998, pp. 70–71).
  - [30] R. G. Gallager, Low-density parity-check codes (MIT Press, Cambridge, MA, 1963).
  - [31] D. MacKay, Good error-correcting codes based on very sparse matrices, *IEEE Trans. Inf. Theory* **45**, 399 (1999).
  - [32] D. Poulin and Y. Chung, On the iterative decoding of sparse quantum codes, *Quant. Inf. Comput.* **8**, 987 (2008).
  - [33] P. Panteleev and G. Kalachev, Degenerate quantum LDPC codes with good finite length performance, e-print arXiv:1904.02703 (2019).
  - [34] J. Roffe, D. R. White, S. Burton, and E. T. Campbell, Decoding across the quantum LDPC code landscape, e-print arXiv:2005.07016 (2020).
  - [35] N. Raveendran and B. Vasić, Trapping sets of quantum LDPC codes, e-print arXiv:2012.15297 (2020).
  - [36] G. Torlai and R. G. Melko, Neural decoder for topological codes, *Phys. Rev. Lett.* **119**, 030501 (2017).
  - [37] S. Krastanov and L. Jiang, Deep neural network probabilistic decoder for stabilizer codes, *Scientific Reports* **7**, 11003 (2017).
  - [38] Y.-H. Liu and D. Poulin, Neural belief-propagation decoders for quantum error-correcting codes, *Phys. Rev. Lett.* **122**, 200501 (2019).
  - [39] N. Maskara, A. Kubica, and T. Jochym-O'Connor, Advantages of versatile neural-network decoding for topological codes, *Phys. Rev. A* **99**, 052351 (2019).
  - [40] J. Bruck and M. Blaum, Neural networks, error-correcting codes, and polynomials over the binary  $n$ -cube, *IEEE Trans. Inf. Theory* **35**, 976 (1989).
  - [41] J. S. Yedidia, W. T. Freeman, and Y. Weiss, Constructing free-energy approximations and generalized belief propagation algorithms, *IEEE Trans. Inf. Theory* **51**, 2282 (2005).
  - [42] R. Lucas, M. Bossert, and M. Breitbart, On iterative soft-decision decoding of linear binary block codes and product codes, *IEEE J. Sel. Areas Commun.* **16**, 276 (1998).
  - [43] J. J. Hopfield, Neurons with graded response have collective computational properties like those of two-state neurons, *Proc. Nat. Acad. Sci. (PANS)* **81**, 3088 (1984).
  - [44] J. J. Hopfield and D. W. Tank, “neural” computation of decisions in optimization problems, *Biological Cybernetics* **52**, 141 (1985).
  - [45] J. J. Hopfield and D. W. Tank, Computing with neural circuits: A model, *Science* **233**, 625 (1986).
  - [46] D. E. Van den Bout and T. K. Miller, Improving the performance of the Hopfield-Tank neural network through normalization and annealing, *Biological Cybernetics* **62**, 129 (1989).
  - [47] C. M. Marcus, F. R. Waugh, and R. M. Westervelt, Non-linear dynamics and stability of analog neural networks, *Physica D* **51**, 234 (1991).
  - [48] J. Wootton and D. Loss, High threshold error correction for the surface code, *Phys. Rev. Lett.* **109**, 160503 (2012).
  - [49] E. Nachmani, E. Marciano, L. Lugosch, W. J. Gross, D. Burshtein, and Y. Be’ery, Deep learning methods for improved decoding of linear codes, *IEEE J. Sel. Topics Signal Process.* **12**, 119 (2018).
  - [50] M. Hagiwara, M. P. C. Fossorier, and H. Imai, Fixed initialization decoding of LDPC codes over a binary symmetric channel, *IEEE Trans. Inf. Theory* **58**, 2321 (2012).
  - [51] I. Sutskever, J. Martens, G. Dahl, and G. Hinton, On

- the importance of initialization and momentum in deep learning, in *Proc. Int. Conf. Mach. Learn. (ICML)* (2013) pp. 1139–1147.
- [52] K.-Y. Kuo, I.-C. Chern, and C.-Y. Lai, Decoding of quantum data-syndrome codes via belief propagation, e-print arXiv:2102.01984 (2021).
  - [53] R. Laflamme, C. Miquel, J. P. Paz, and W. H. Zurek, Perfect quantum error correcting code, *Phys. Rev. Lett.* **77**, 198 (1996).
  - [54] M. Fossorier and S. Lin, Soft-decision decoding of linear block codes based on ordered statistics, *IEEE Trans. Inf. Theory* **41**, 1379 (1995).
  - [55] S. Bravyi, M. Suchara, and A. Vargo, Efficient algorithms for maximum likelihood decoding in the surface code, *Phys. Rev. A* **90**, 032326 (2014).
  - [56] N. Delfosse and N. H. Nickerson, Almost-linear time decoding algorithm for topological codes, e-print arXiv:1709.06218 (2017).
  - [57] B. Criger and I. Ashraf, Multi-path summation for decoding 2D topological codes, *Quantum* **2**, 102 (2018).
  - [58] H. Bombin, R. Andrist, M. Ohzeki, H. Katzgraber, and M. Martín-Delgado, Strong resilience of topological codes to depolarization, *Phys. Rev. X* **2**, 021004 (2012).
  - [59] M. Ohzeki, Error threshold estimates for surface code with loss of qubits, *Phys. Rev. A* **85**, 060301 (2012).
  - [60] Additional stabilizers ( $M > N - K$ ) may provide stronger protection, e.g., a toric code has every qubit equally protected by four stabilizers due to additional stabilizers. In the case that the syndrome measurement operations are faulty, we may need to measure additional stabilizers to obtain reliable syndrome information [52, 88].
  - [61] R. Tanner, A recursive approach to low complexity codes, *IEEE Trans. Inf. Theory* **27**, 533 (1981).
  - [62] N. Wiberg, *Codes and decoding on general graphs*, Ph.D. thesis, Linköping University, Linköping, Sweden (1996).
  - [63] J. Pearl, *Probabilistic reasoning in intelligent systems: networks of plausible inference* (Kaufmann, 1988).
  - [64] F. R. Kschischang, B. J. Frey, and H.-A. Loeliger, Factor graphs and the sum-product algorithm, *IEEE Trans. Inf. Theory* **47**, 498 (2001).
  - [65] R. J. McEliece, D. J. C. MacKay, and J.-F. Cheng, Turbo decoding as an instance of Pearl’s “belief propagation” algorithm, *IEEE J. Sel. Areas Commun.* **16**, 140 (1998).
  - [66] S. M. Aji and R. J. McEliece, The generalized distributive law, *IEEE Trans. Inf. Theory* **46**, 325 (2000).
  - [67] J. Chen and M. P. C. Fossorier, Density evolution for two improved BP-based decoding algorithms of LDPC codes, *IEEE Commun. Lett.* **6**, 208 (2002).
  - [68] J. Chen, A. Dholakia, E. Eleftheriou, M. P. C. Fossorier, and X.-Y. Hu, Reduced-complexity decoding of LDPC codes, *IEEE Trans. Commun.* **53**, 1288 (2005).
  - [69] Y.-J. Wang, B. C. Sanders, B.-M. Bai, and X.-M. Wang, Enhanced feedback iterative decoding of sparse quantum codes, *IEEE Trans. Inf. Theory* **58**, 1231 (2012).
  - [70] M. Reimpell and R. F. Werner, Iterative optimization of quantum error correcting codes, *Phys. Rev. Lett.* **94**, 080501 (2005).
  - [71] Sometimes we encounter the curve fluctuation as in Figs. 5, 6 or 10 (a). Using a fixed  $\epsilon_0$  for initialization can improve this. This can be proved by the theory in [50]. Put it more simply: if BP has  $r \times$  BDD performance at some  $\epsilon$ , then most errors within the corresponding correction radius would be correctable by BP. Using a fixed  $\epsilon_0$  at this  $\epsilon$  enables BP to have the performance curve interpolated or extrapolated without fluctuation.
  - [72] T. Richardson, M. Shokrollahi, and R. Urbanke, Design of capacity-approaching irregular low-density parity-check codes, *IEEE Trans. Inf. Theory* **47**, 619 (2001).
  - [73] V. Rathi and R. Urbanke, Density evolution, thresholds and the stability condition for non-binary LDPC codes, *IEE Proceedings-Communications* **152**, 1069 (2005).
  - [74] S. ten Brink, Convergence behavior of iteratively decoded parallel concatenated codes, *IEEE Trans. Commun.* **49**, 1727 (2001).
  - [75] A. Ashikhmin, G. Kramer, and S. ten Brink, Extrinsic information transfer functions: model and erasure channel properties, *IEEE Trans. Inf. Theory* **50**, 2657 (2004).
  - [76] G. Lechner and J. Sayir, Improved sum-min decoding for irregular LDPC codes, in *Proc. Int. Symp. Turbo Codes and Related Topics* (2006) pp. 1–6.
  - [77] J. Chen and M. P. C. Fossorier, Near optimum universal belief propagation based decoding of low-density parity check codes, *IEEE Trans. Commun.* **50**, 406 (2002).
  - [78] M. Sipser and D. A. Spielman, Expander codes, *IEEE Trans. Inf. Theory* **42**, 1710 (1996).
  - [79] M. P. C. Fossorier, M. Mihaljevic, and H. Imai, Reduced complexity iterative decoding of low-density parity check codes based on belief propagation, *IEEE Trans. Commun.* **47**, 673 (1999).
  - [80] D. S. Wang, A. G. Fowler, C. D. Hill, and L. C. L. Hollenberg, Graphical algorithms and threshold error rates for the 2d color code, *Quant. Inf. Comput.* **10**, 780 (2010).
  - [81] H. Bombin, G. Duclos-Cianci, and D. Poulin, Universal topological phase of two-dimensional stabilizer codes, *New J. Phys.* **14**, 073048 (2012).
  - [82] N. Delfosse, Decoding color codes by projection onto surface codes, *Phys. Rev. A* **89**, 012317 (2014).
  - [83] P. Sarvepalli and R. Raussendorf, Efficient decoding of topological color codes, *Phys. Rev. A* **85**, 022317 (2012).
  - [84] A. M. Stephens, Efficient fault-tolerant decoding of topological color codes, e-print arXiv:1402.3037 (2014).
  - [85] A. Grospellier, L. Grouès, A. Krishna, and A. Leverrier, Combining hard and soft decoders for hypergraph product codes, *Quantum* **5**, 432 (2021).
  - [86] A. Leverrier, J.-P. Tillich, and G. Zémor, Quantum expander codes, in *Proc. Annu. Symp. Found. Comput. Sci. (FOCS)* (IEEE, 2015) pp. 810–824.
  - [87] O. Fawzi, A. Grospellier, and A. Leverrier, Efficient decoding of random errors for quantum expander codes, in *Proc. Annu. ACM SIGACT Symp. Theory Comput. (STOC)* (2018) pp. 521–534.
  - [88] A. Ashikhmin, C.-Y. Lai, and T. A. Brun, Quantum data-syndrome codes, *IEEE J. Sel. Areas Commun.* **38**, 449 (2020).